RADIO DIRECTION FINDING (RDF) - GEOMAGNETIC MONITORING STUDY OF THE JAPANESE AREA RELATED TO PRE-SEISMIC ELECTROMAGNETIC SIGNALS

Valentino Straser
Department of Science and Environment UPKL, Brussels – (valentino.straser@gmail.com)

Daniele Cataldi
Radio Emissions Project, Rome (Italy) – (daniele77c@gmail.com)

Gabriele Cataldi
Radio Emissions Project, Rome (Italy) – (ltpaobserverproject@gmail.com)

Abstract: The study aims to present data relating to broadband electromagnetic monitoring (SELF-VLF band, 0-32000 Hz) capable of working 24/7, within the electromagnetic monitoring network with RDF (Radio Direction Finding) technology. The area monitored area for experimentation is the Japanese one, historically affected by strong and devastating earthquakes. The study found 1424 groups of radio anomalies, related to crustal diagnosis and non-destructive earthquakes. This is the first network of this type capable of working on a wide bandwidth (ELF-VLF band, 0-96000 Hz) specially designed to study the so-called "Seismic Electromagnetic Precursors" (SEPs) and the "Seismic Geomagnetic Precursors" "(SGPs). This monitoring system, based on RDF technology, has been active since 2017.

Keywords: RDF system, earthquake prediction, SELF-VLF, Japanese area, earthquake.

1 – INTRODUCTION

The system developed by the Radio Emissions Project, based on RDF - Radio Direction Finding technology, has made it possible to ascertain from 2017 the existence of strong electromagnetic signals before the occurrence of an earthquake (Straser et al., 2018; Straser et al., 2017; Straser et al., 2016; Straser et al., 2015, Cataldi et al. 2017, Cataldi et al. 2016). On 24 January 2019, monitoring began of the Japanese area, an area characterized by very strong earthquakes and high seismic risk, not least that of 11 March 2011 of magnitude Mw9 which caused extreme disasters in north-eastern Japan due to the high waves of a tsunami generated by the earthquake and the strong movements of the soil. The death toll and missing persons were estimated at over 20,000. Before this earthquake occurred, for more than 30 years on the border between the Pacific and the North American plates, no other destructive earthquakes had occurred, after that of Miyagi in 1978, it was therefore expected that there would be a strong earthquake within 30 years subsequent, with a probability of 99% and this happened (Furumura et al., 2011). This monitoring was used to ascertain the appearance of any electromagnetic signals that appeared before a possible strong earthquake, to understand if there were evident electromagnetic phenomena that could have indicated crustal energy accumulation phenomena, typical of the area subjected to electromagnetic monitoring.

2 – INSTRUMENT

2.1 – The RDF Station in Lariano (Rome, Italy)

The RDF (Radio Direction Finding) station used for this study is that of Lariano (Rome, Italy; Lat: 41.729535N, Long: 12.840968E), equipped with two Loop antennas with a diameter of 1 meter containing 50 turns each (Fig.1), aligned with each other orthogonally and with respect to the geographical poles.

It is managed by Daniele Cataldi and is equipped with a radio receiver prototype designed and built by Gabriele Cataldi which is able to detect changes in the electromagnetic field in the VLF band (0.3-96 kHz) 24/7.

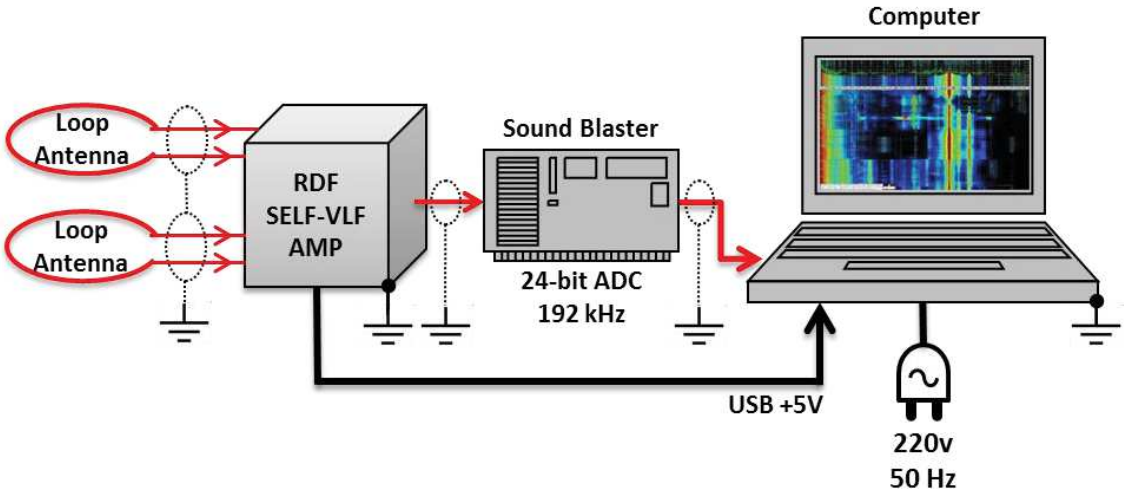

Fig. 1 - Schematization of the RDF Radio Direction Finding receiving and amplification system located in Lariano, Rome, Italy; developed by the Radio Emissions Project, and used for this study. It consists of two Loop antennas, a radio amplifier (receiver), connected to the PC's microphone socket, via the Sound Blaster.

3 – THE STUDY

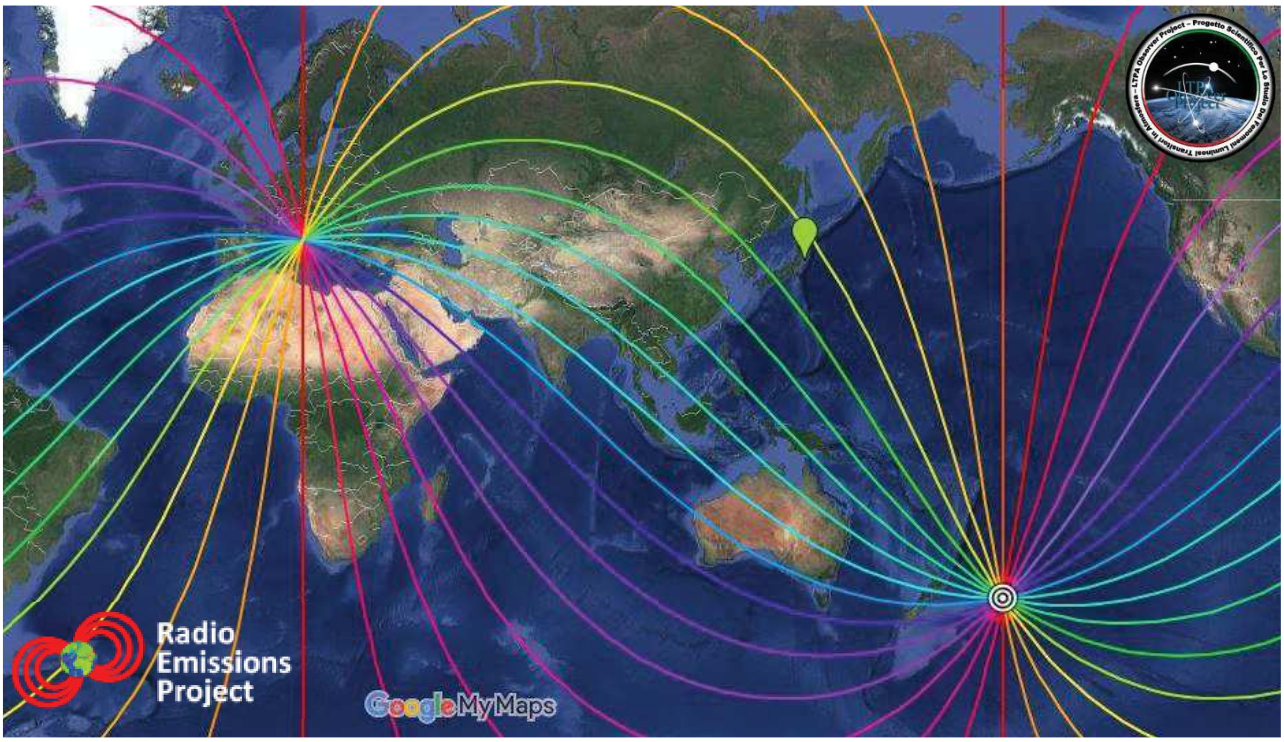

Fig. 2 – Monitoring area

On January 24, 2019, electromagnetic monitoring of the Japanese area began, as visible in Fig. 2 and 3, continuing until October 14, 2019. This electromagnetic monitoring was made possible thanks to the RDF - Radio Direction Finding station of the electromagnetic detection system of the Radio Emissions Project in Lariano, Rome, Italy.

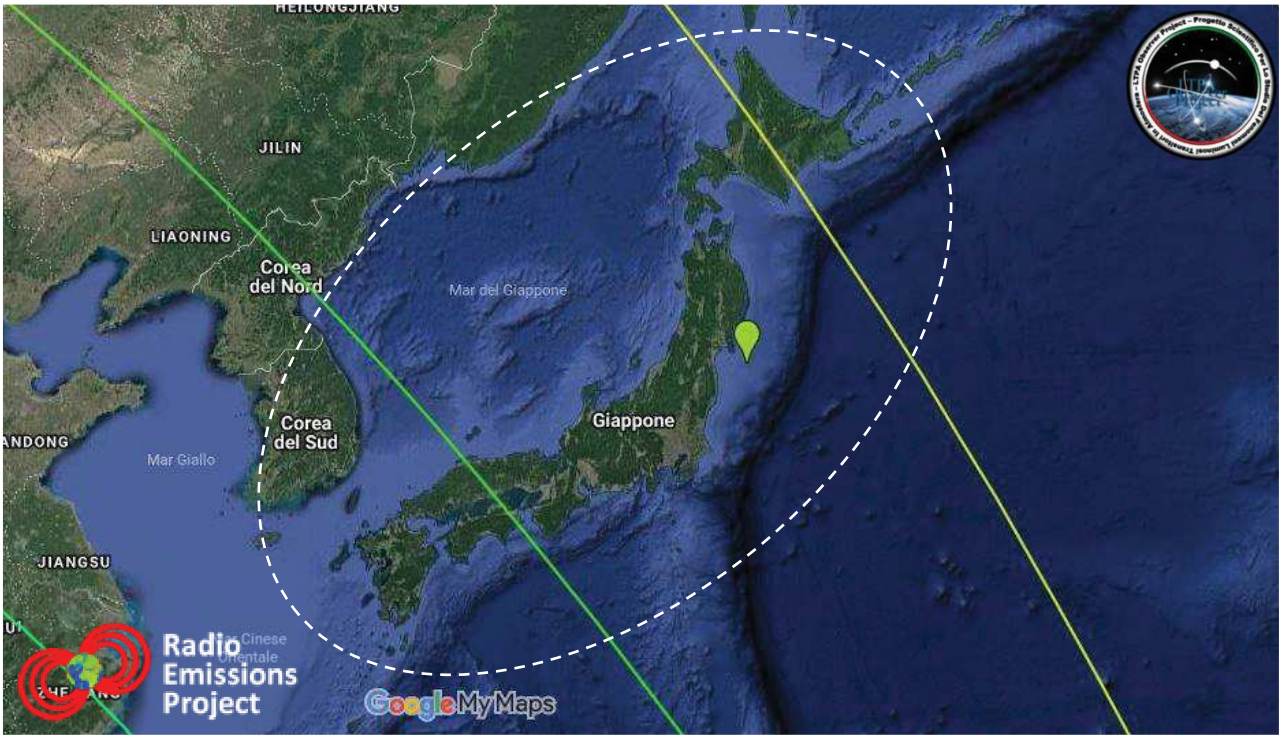

Fig. 3 - The geographical area examined and the azimuth monitored by the RDF system of Lariano, Rome, Italy and Pontedera, Pisa, Italy.

The monitored area is about 9,800 km from the RDF station (Rome, Italy), as shown in Fig. 5. This distance, considering the reception characteristics of the RDF station itself, is not to be underestimated compared to the total coverage of the station (with a radius of 20,000 km), reaching about half of the maximum coverage (in this case the experimentation took place in 2017) (Straser et al., 2018), as seen in Fig. 4

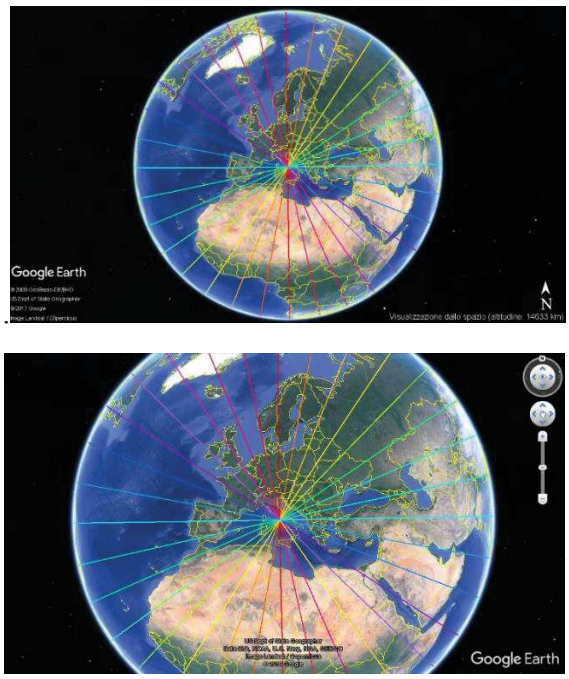

Fig. 4 - Worldwide coverage of the RDF system, developed by Daniele and Gabriele Cataldi.

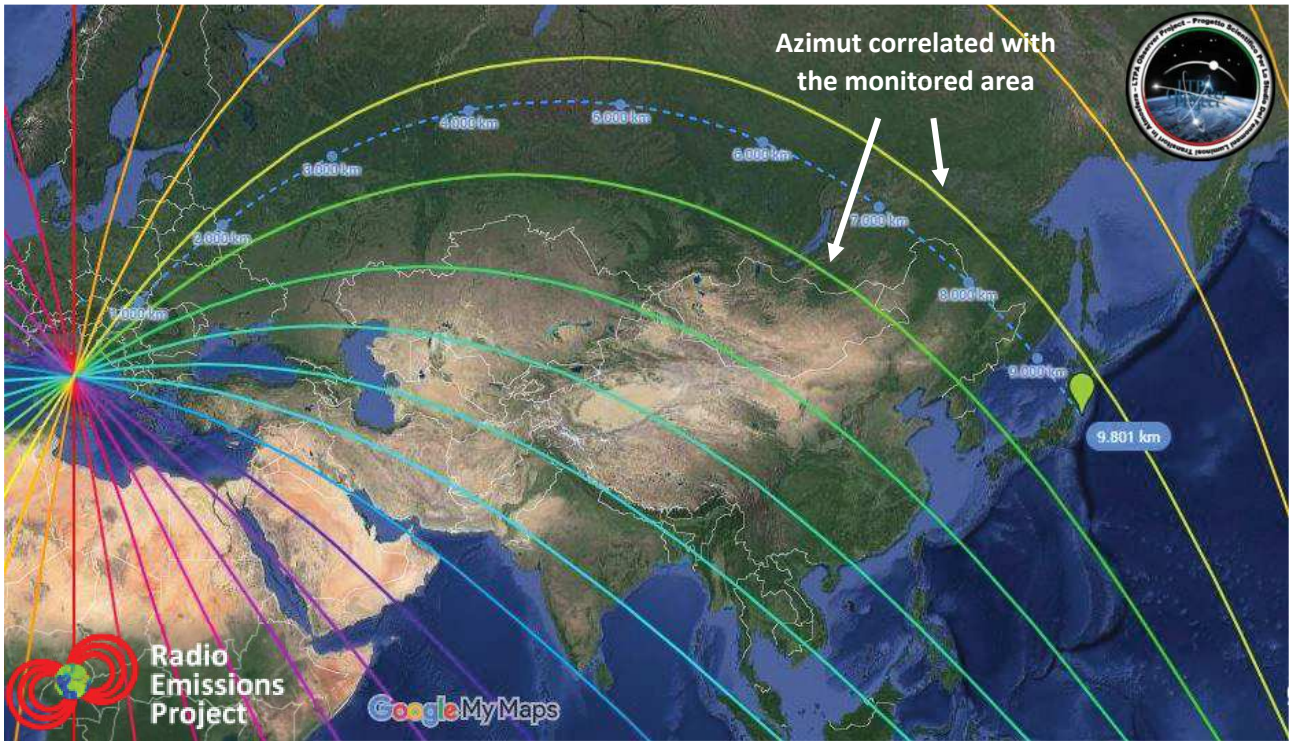

Fig. 4 - Distance between Lariano RDF station, Rome, Italy and the monitored Japanese area. Google Maps.

In this case, the monitored electromagnetic signals fall under the green and yellow azimuth, including the relative nuances, as highlighted by the colorimetric map of the RDF system in Lariano (RM) (Fig. 5). This azimuth is located in the NE - NNE direction with respect to the Italian geographical position in which the RDF monitoring station is located. This geographical area is extremely large (as visible in Fig. 3):

• Perimeter: 5,862 km

• Area: 1,983,373,034 km2

The monitoring system therefore had to keep under continuous electromagnetic control all the emissions from this large area, also considering the proximity to the ring of fire, which is a few thousand kilometers away and which appears to be a very large natural emitter of emissions electromagnetic continuous and strong intensity. The signals coming from this large area have often generated intense electromagnetic modulations, such as to cover the weak emissions coming from the Japanese territory.

This is therefore one of the important data not to be underestimated, which was however considered in this study and which represented a "limit" of the RDF system, in detecting further signals from the area under continuous monitoring data.

4 –DATA

4.1 – The Signals

The signals recorded by the RDF - Radio Direction Finding system, developed by the Radio Emissions Project, concerned pulsing or continuous increases in correspondence with the green / yellow azimuth, these signals appeared very frequently, saturating, sometimes part of the apparitions, the The entire

electromagnetic band taken into consideration (0-96 kHz of bandwidth), as shown in Fig. 6. In this case the number of dynamic spectrograms investigated and generated by the system were 447.

Sporadic signals instead appeared only at certain frequencies, whose emission characteristics are discussed in this study.

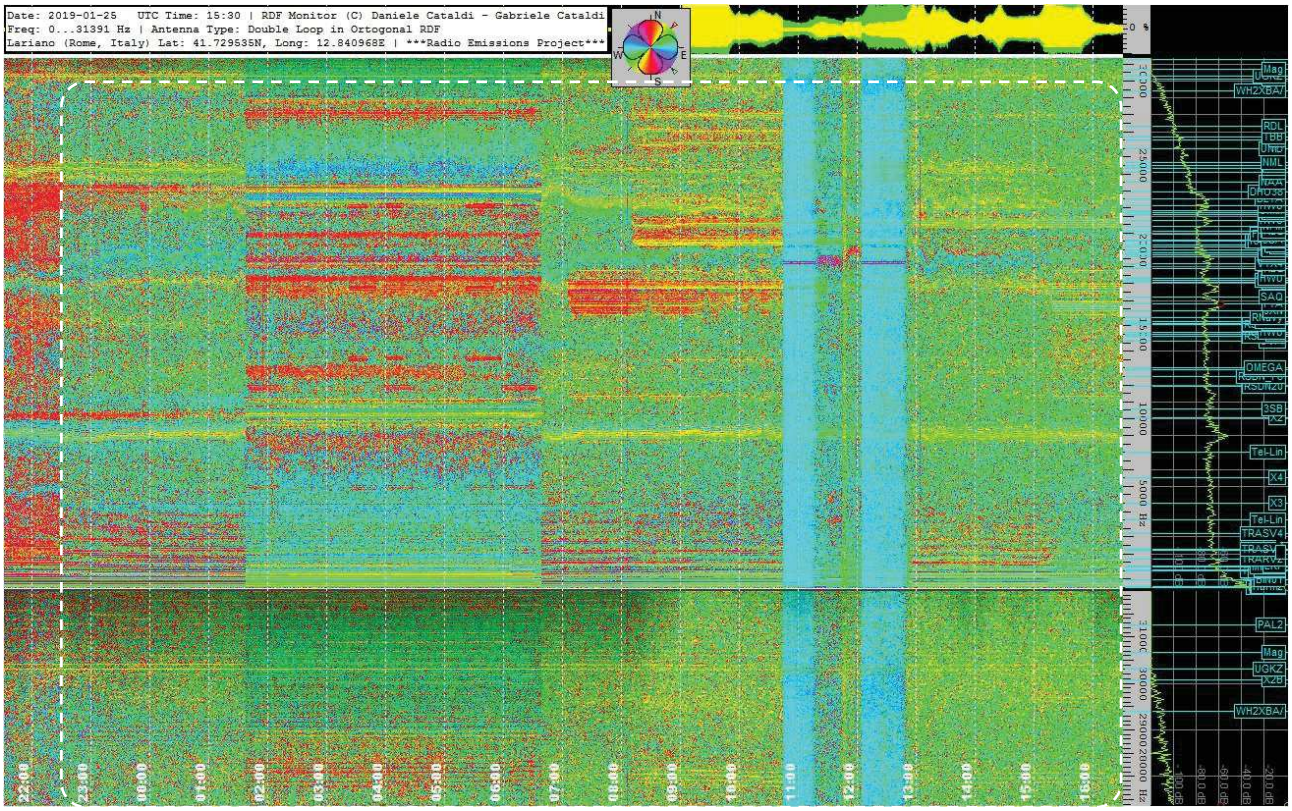

Fig. 5 - An example of the greeen/yellow signals (radio-anomaly) recorded, coming from japanese azimuth. In this case it is one of the spectrograms recorded by the RDF station in Lariano, Rome, Italy.

The study undertaken by the Radio Emissions Project through the RDF station in Lariano, Rome, Italy, highlighted some interesting characteristics of the radio anomalies recorded during the study, a study focused on the search for signals having seismic predictive characteristics in the Japanese area.

The signals considered were only those polarized with the Japanese azimuth, eliminating all the increases and electromagnetic peaks coming from other geographical areas of the earth's globe.

The first interesting data are the number of anomalies (having the same azimuth as the area under monitoring), which appeared over the weeks and months in which this study continued.

5 – THE STUDY

The total number of radio anomalies recorded during the study is 1424, each of which correlated with the Japanese azimuth. This number is associated with electromagnetic increases having different frequencies (as visible in Fig. 7, 8, 9, 10, 11, 12, 13, 14, 15, 16). The data contained in this study were extrapolated from the monitoring system developed by Daniele Cataldi and Gabriele Cataldi, which independently detected the electromagnetic emissions, providing indications on their azimuth origin (frequency polarization), in relation to the entire extension of the earth's surface and therefore taking into consideration the geographical areas of the terrestrial globe, from where these signals come.

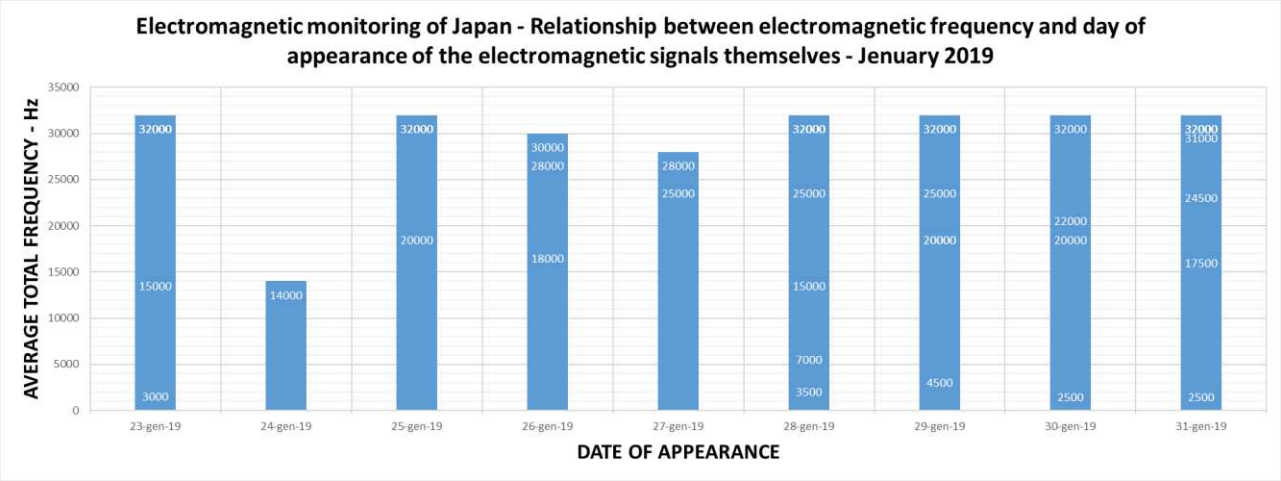

Fig. 6 - Relationship between the number of radio anomalies that appeared during the study and their frequency distribution. Source: Radio Emissions Project. January 2019.

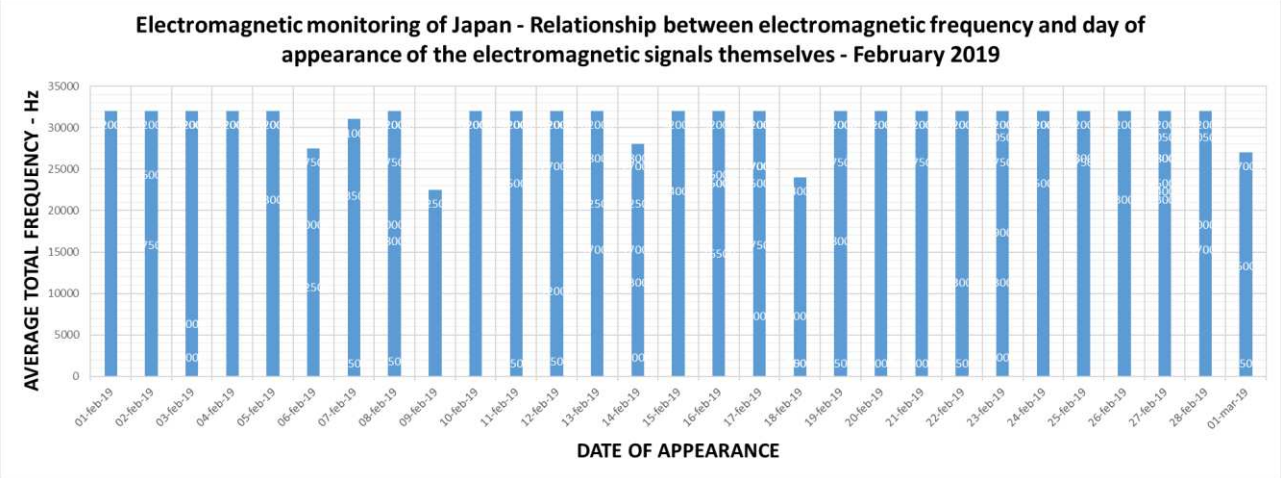

Figure 8 - Relationship between the number of radio anomalies that appeared during the study and their frequency distribution. Source: Radio Emissions Project. February 2019.

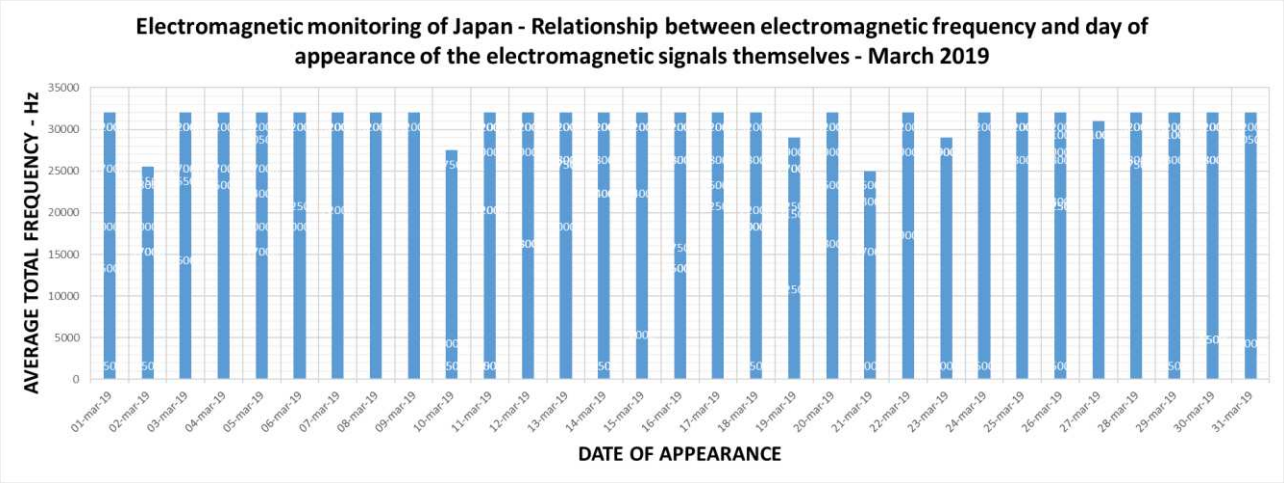

Figure 9 - Relationship between the number of radio anomalies that appeared during the study and their frequency distribution. Source:

Radio Emissions Project. March 2019.

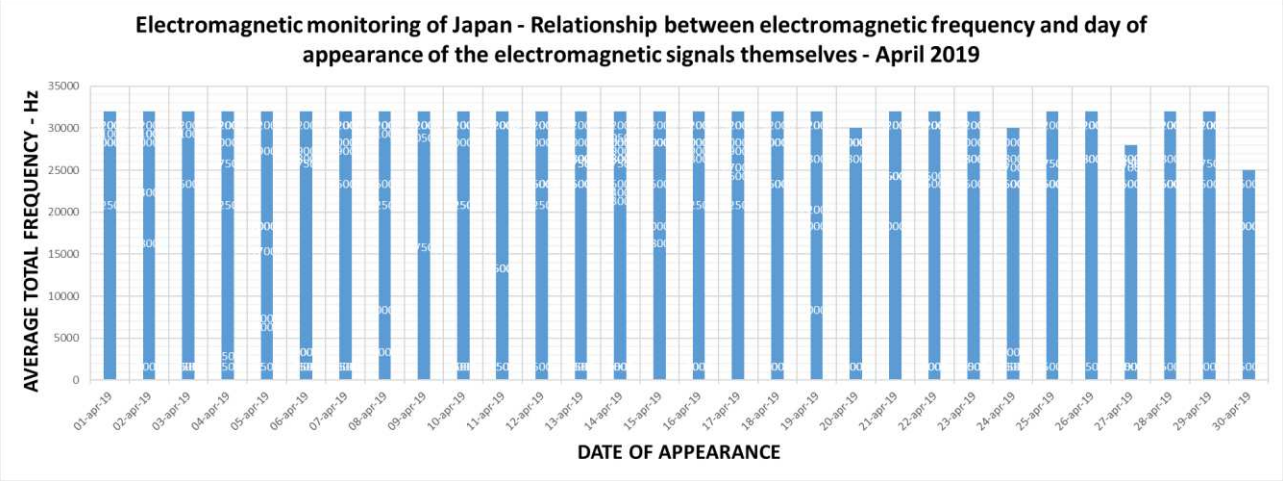

Figure 10 - Relationship between the number of radio anomalies that appeared during the study and their frequency distribution. Source: Radio Emissions Project. April 2019.

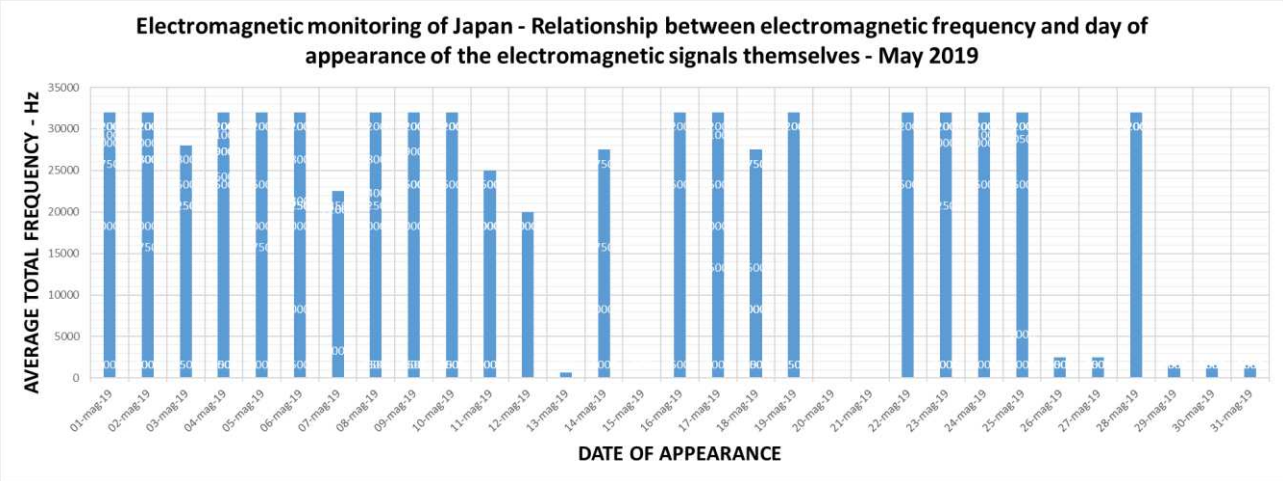

Figure 11 - Relationship between the number of radio anomalies that appeared during the study and their frequency distribution. Source: Radio Emissions Project. May 2019.

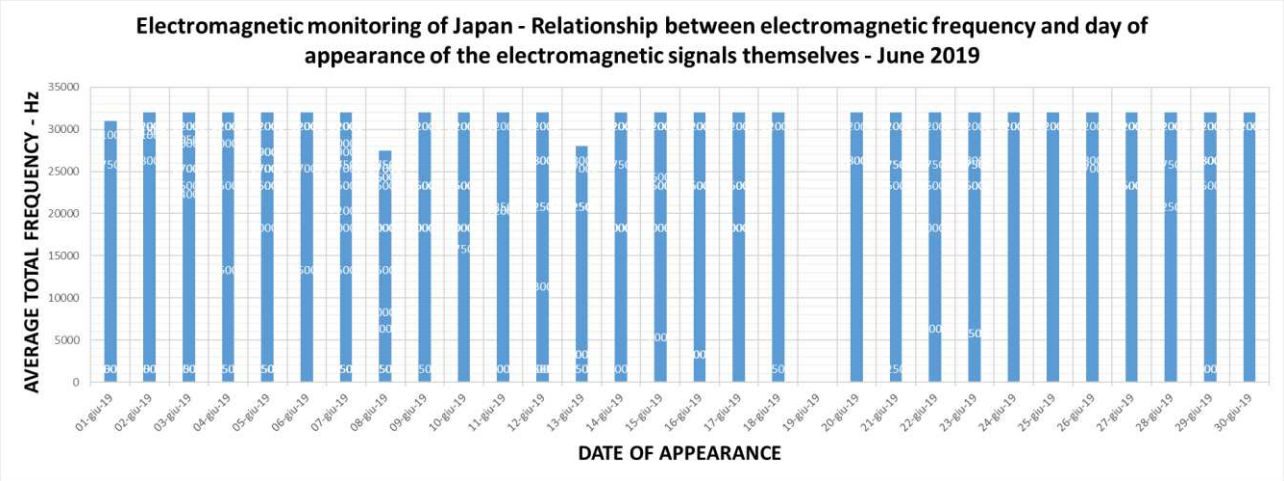

Figure 12 - Relationship between the number of radio anomalies that appeared during the study and their frequency distribution. Source:

Radio Emissions Project. June 2019.

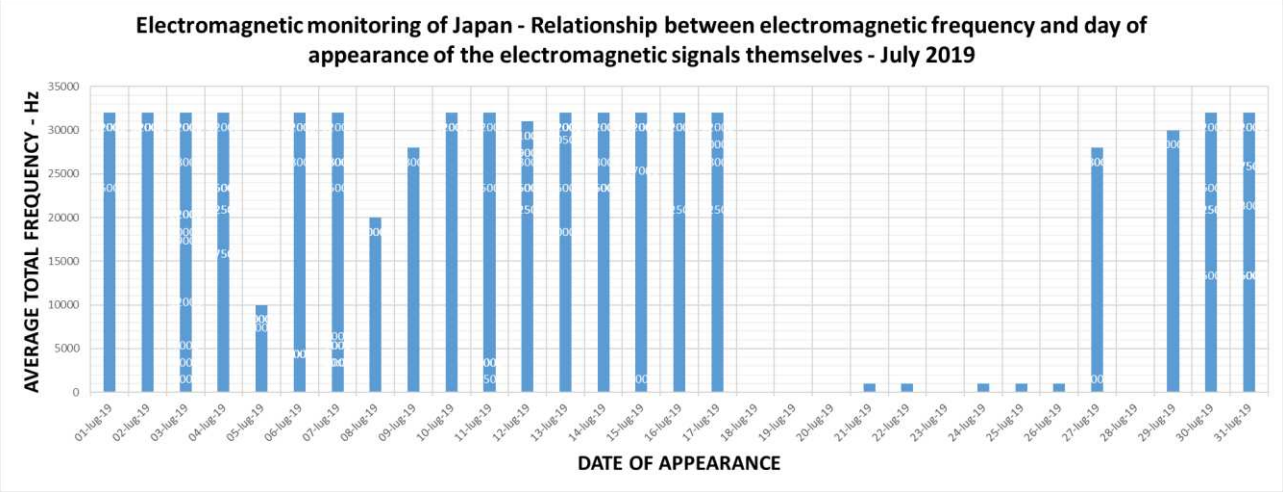

Figure 13 - Relationship between the number of radio anomalies that appeared during the study and their frequency distribution. Source: Radio Emissions Project. July 2019.

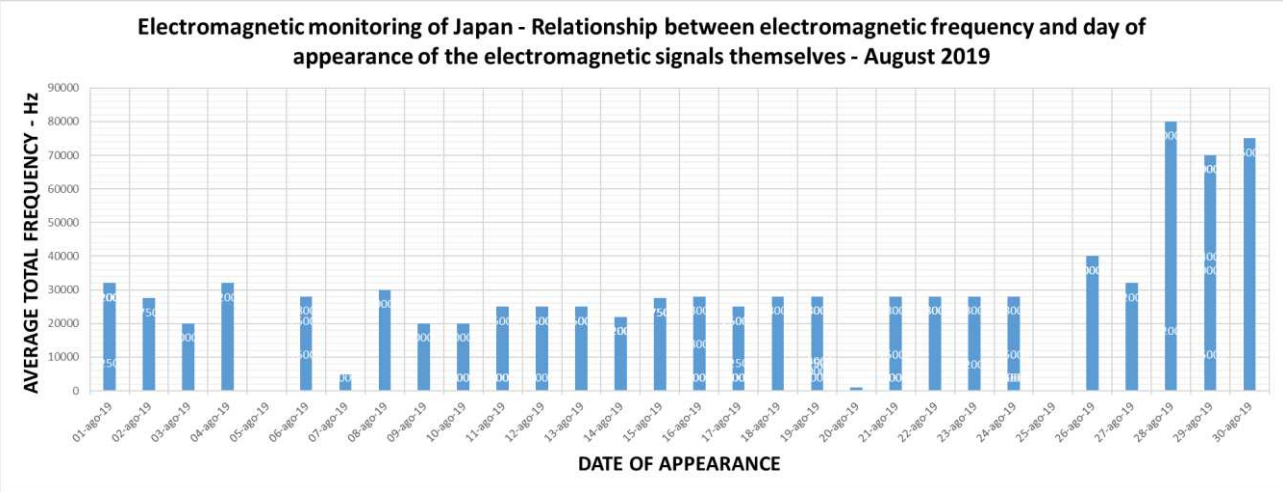

Figure 14 - Relationship between the number of radio anomalies that appeared during the study and their frequency distribution. Source: Radio Emissions Project. August 2019.

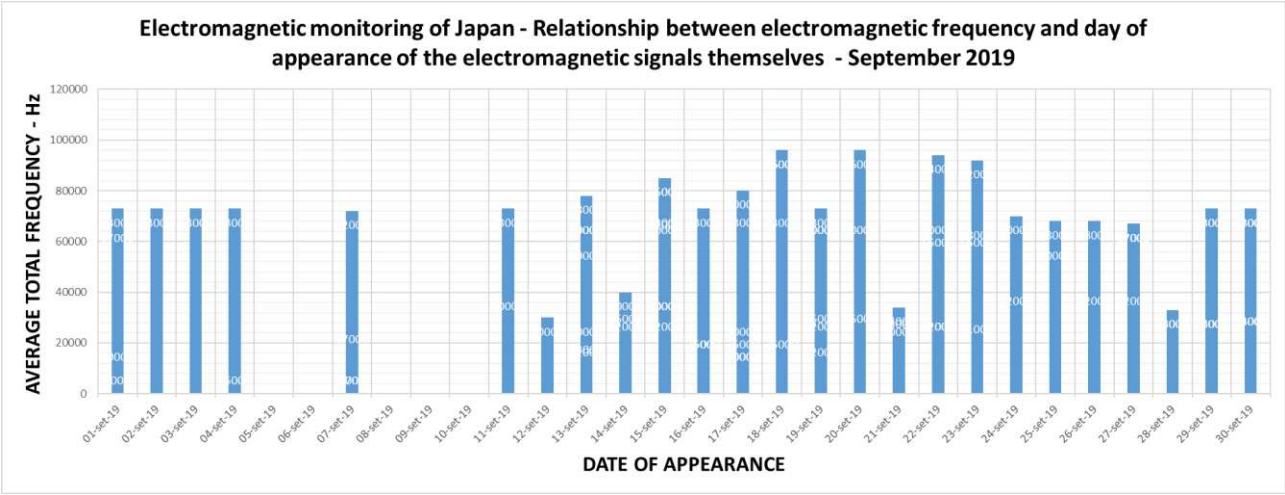

Figure 15 - Relationship between the number of radio anomalies that appeared during the study and their frequency distribution. Source: Radio Emissions Project. September 2019

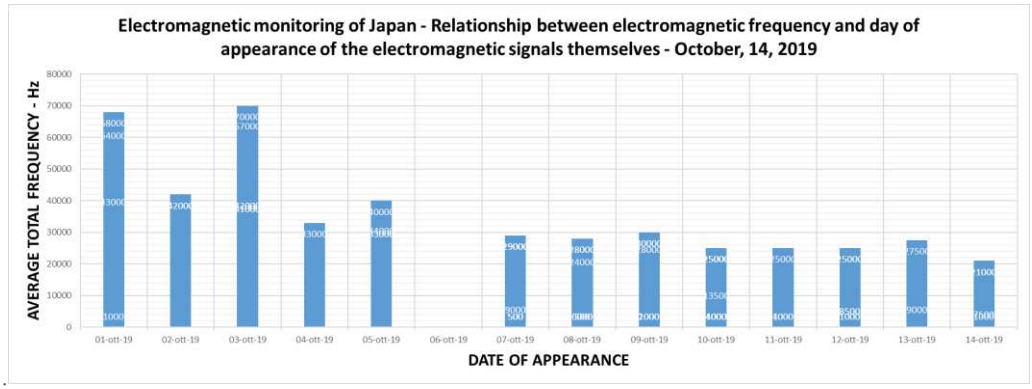

Figure 16 - Relationship between the number of radio anomalies that appeared during the study and their frequency distribution. Source: Radio Emissions Project. October 2019.

The study of the electromagnetic frequency of the radio-anomalies associated with the Japanese azimuth, shows us how there is the majority of electromagnetic emissions distributed over the entire electromagnetic band taken into consideration (0-32,000 Hz), coming from the monitored area.

In this context, it is possible to understand the behavior of these emissions on the time axis (as visible in Fig. 7, 8, 9, 10, 11, 12, 13, 14, 15, 16).

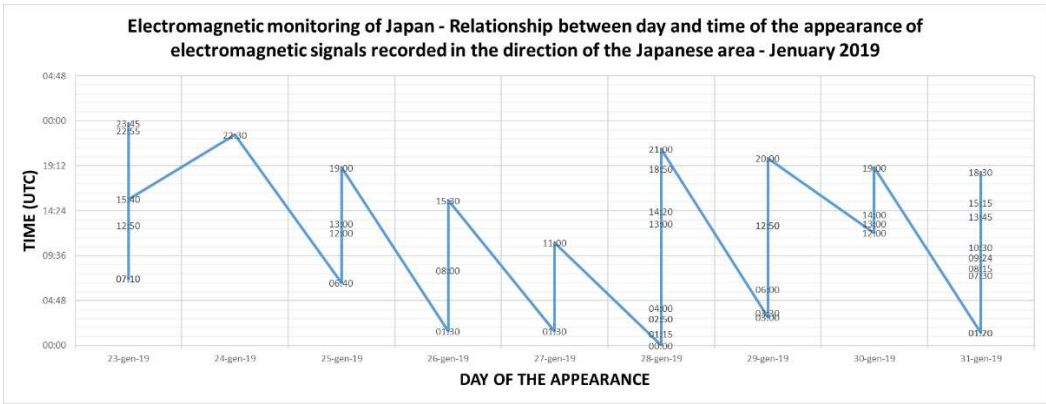

Fig. 17 - Relationship between number of anomalies, date and time of appearance compared to the period considered in the study. Source: Radio Emissions Project. January 2019.

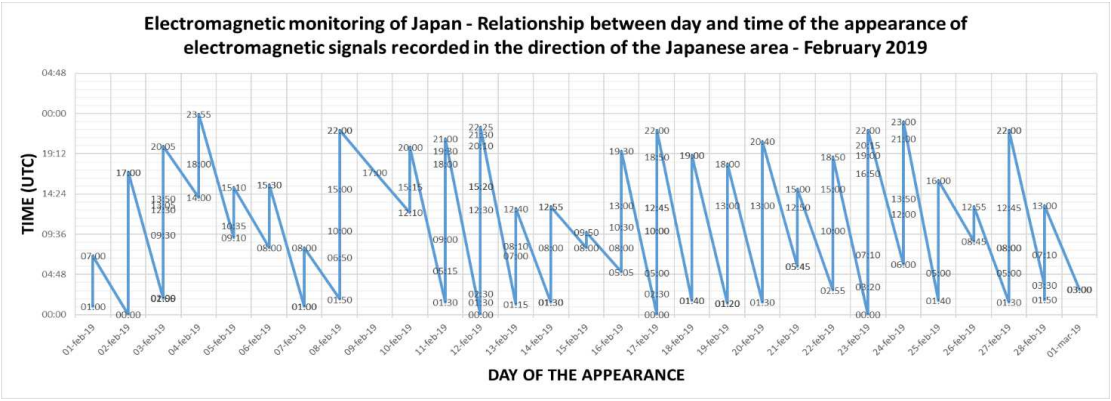

Figure 18 - Relationship between number of anomalies, date and time of appearance compared to the period considered in the study. Source: Radio Emissions Project. February 2019

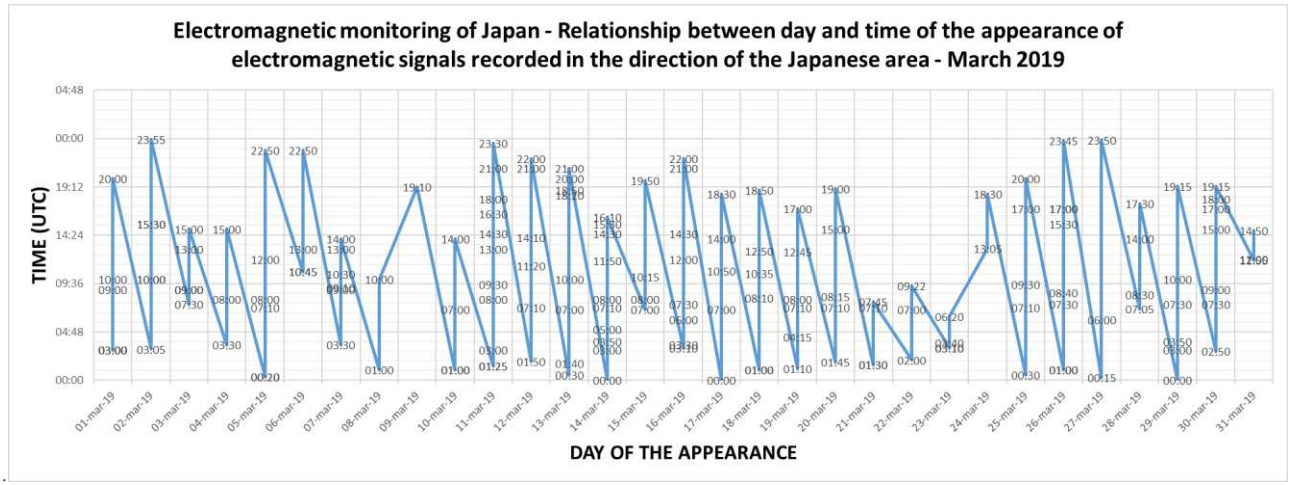

Figure 19 - Relationship between number of anomalies, date and time of appearance compared to the period considered in the study. Source: Radio Emissions Project. March 2019.

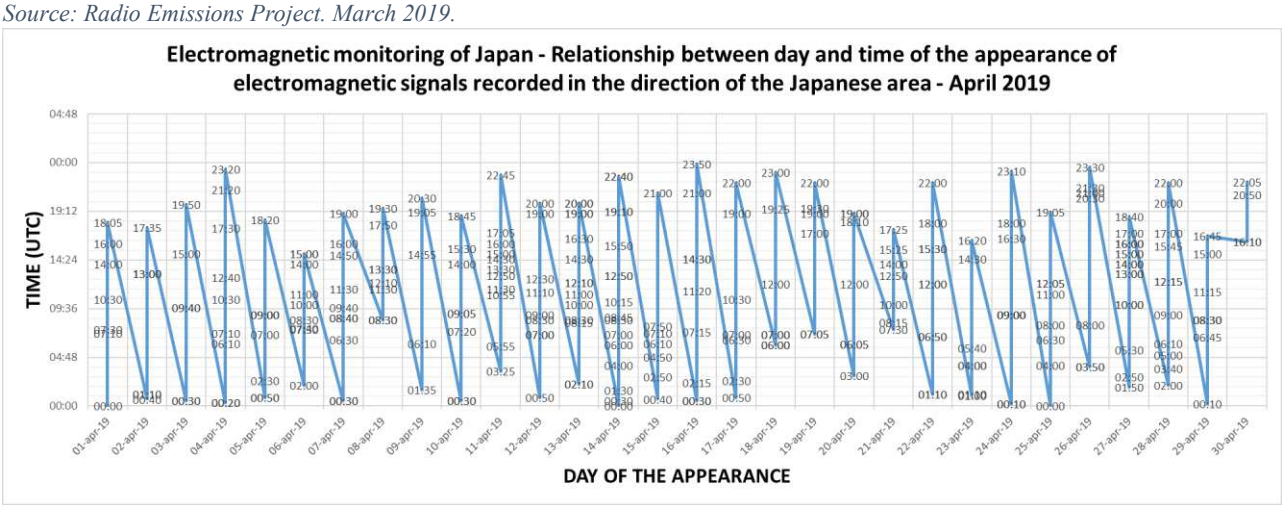

Figure 20 - Relationship between number of anomalies, date and time of appearance compared to the period considered in the study. Source: Radio Emissions Project. April 2019.

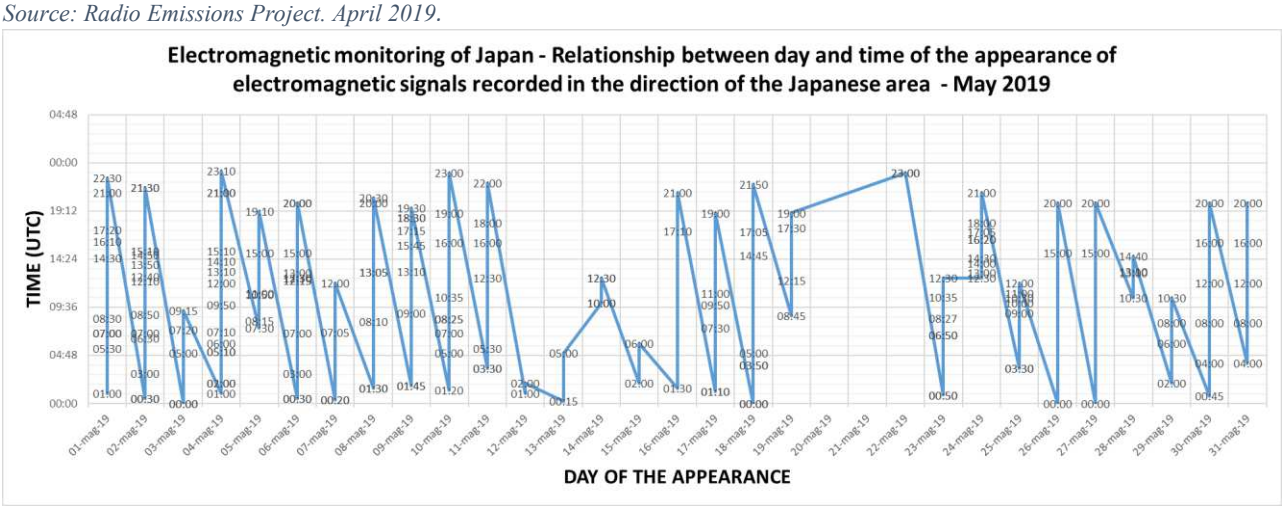

Figure 21 - Relationship between number of anomalies, date and time of appearance compared to the period considered in the study. Source: Radio Emissions Project. May 2019.

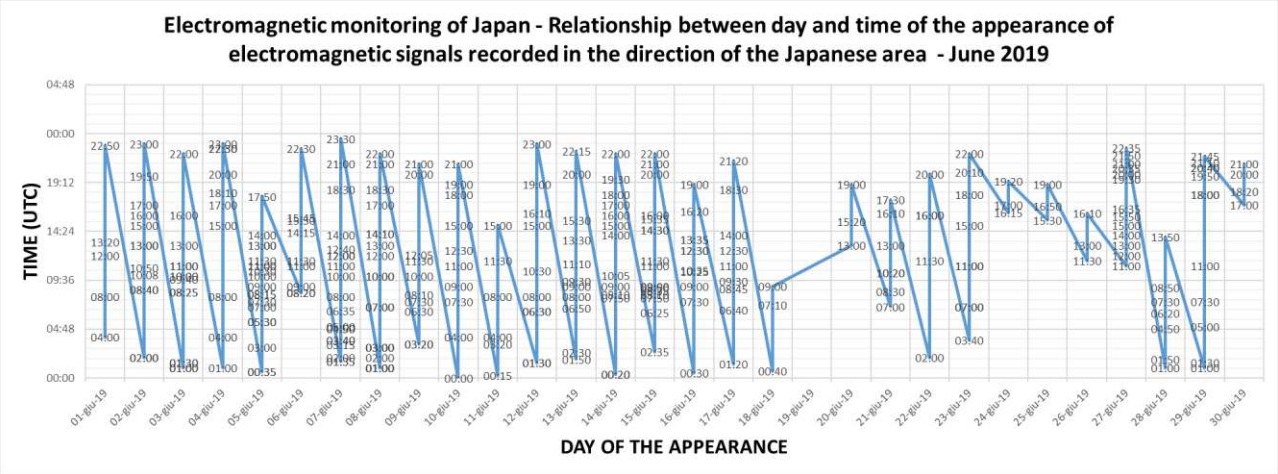

Figura 7 - Relazione tra numero di anomalie, data ed orario di comparsa rispetto al periodo considerato nello studio. Fonte: Radio Emissions Project. Giugno 2019.

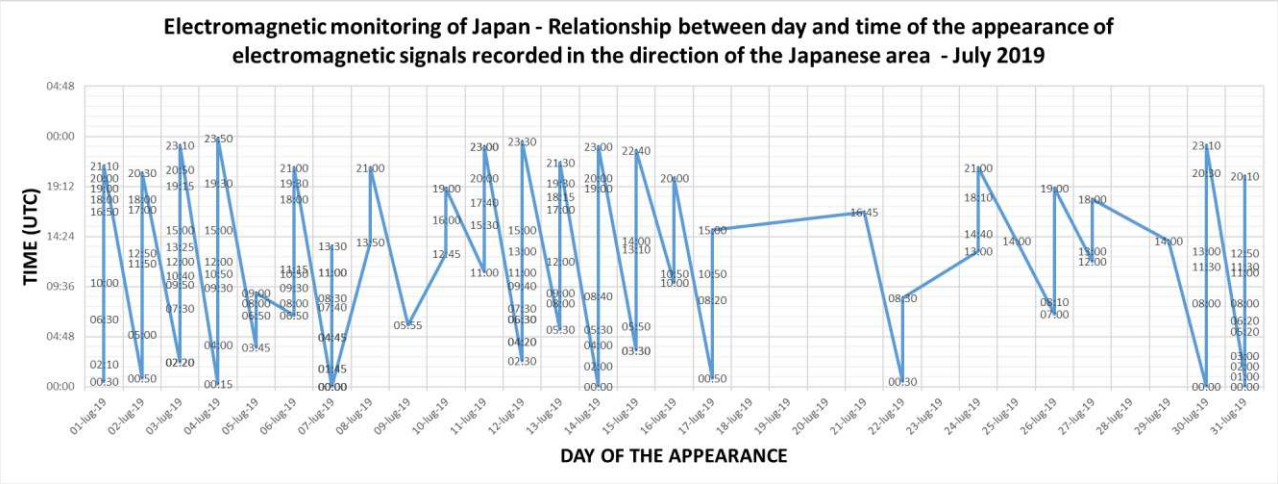

Figure 23 - Relationship between number of anomalies, date and time of appearance compared to the period considered in the study. Source: Radio Emissions Project. July 2019.

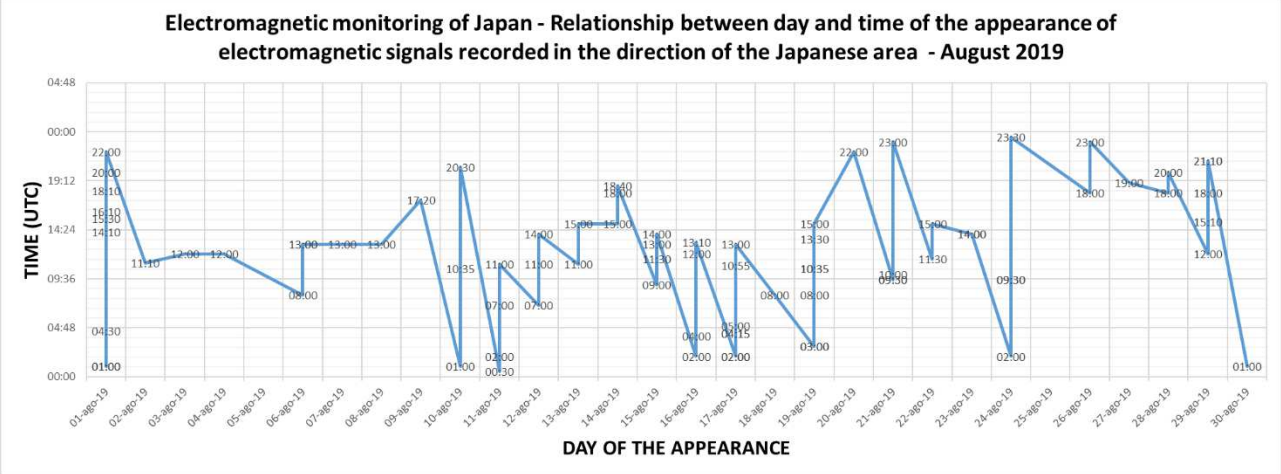

Figure 24 - Relationship between number of anomalies, date and time of appearance compared to the period considered in the study. Source: Radio Emissions Project. August 2019.

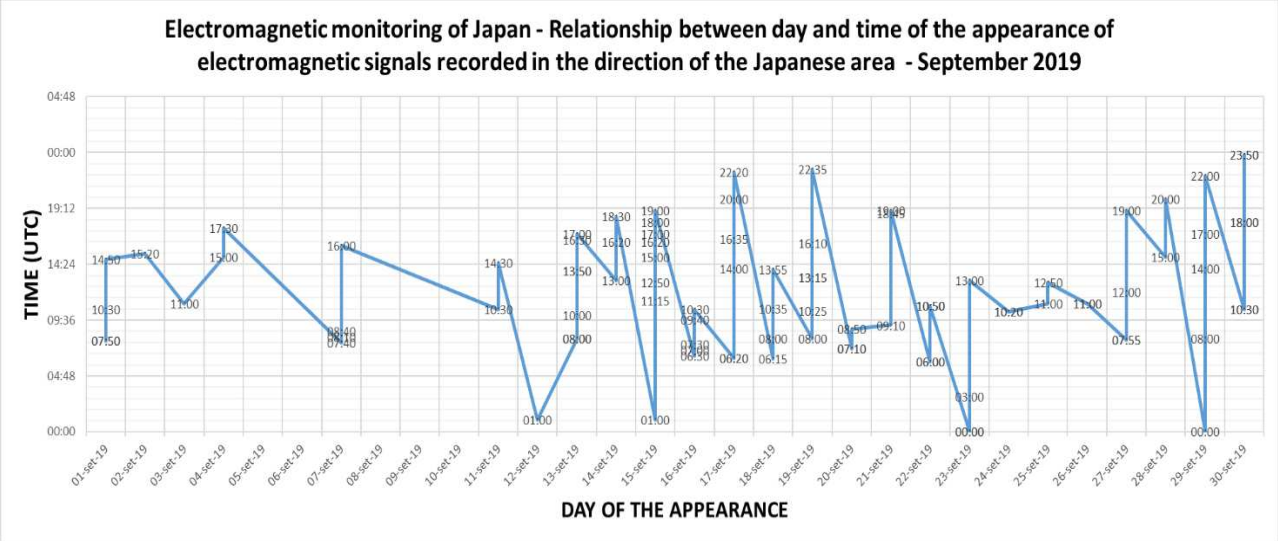

Figure 25 - Relationship between number of anomalies, date and time of appearance compared to the period considered in the study. Source: Radio Emissions Project. September 2019.

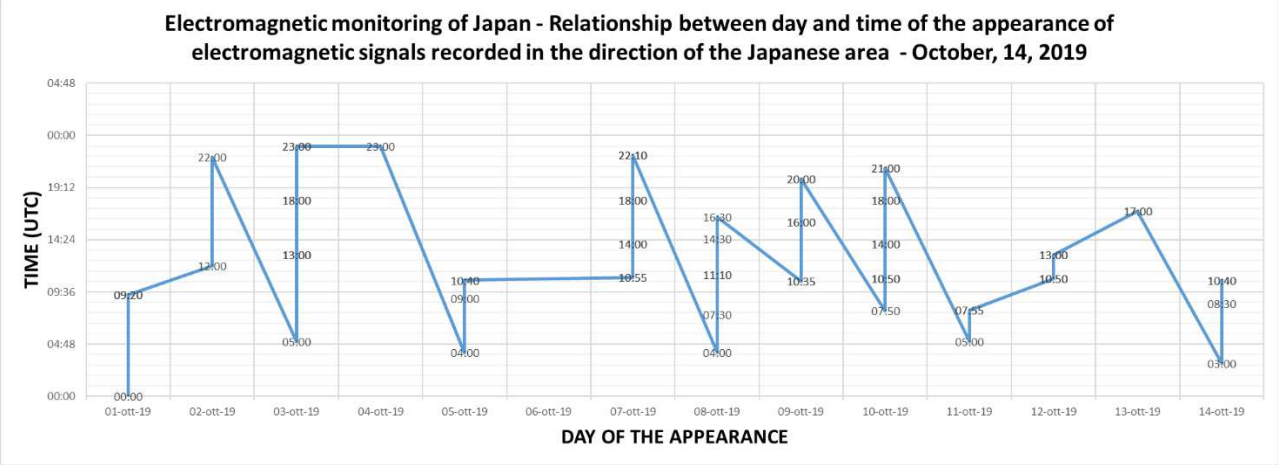

Figure 26 - Relationship between number of anomalies, date and time of appearance compared to the period considered in the study. Source: Radio Emissions Project. October 2019.

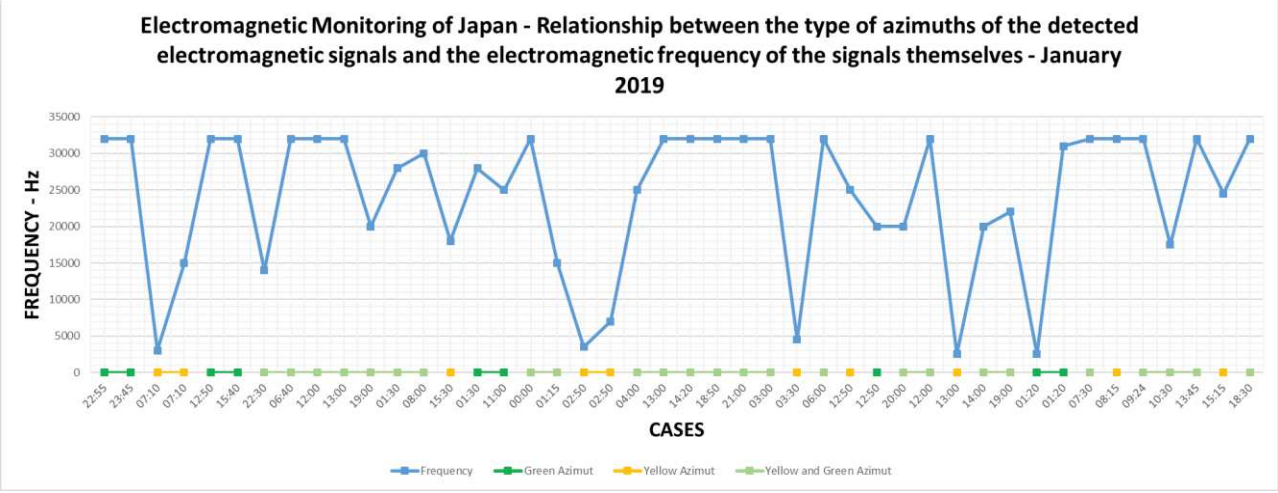

Fig. 27 - Relationship between the electromagnetic frequency of the signals received and their source azimuth. (green, green / yellow, yellow). Source: Radio Emissions Project. January 2019.

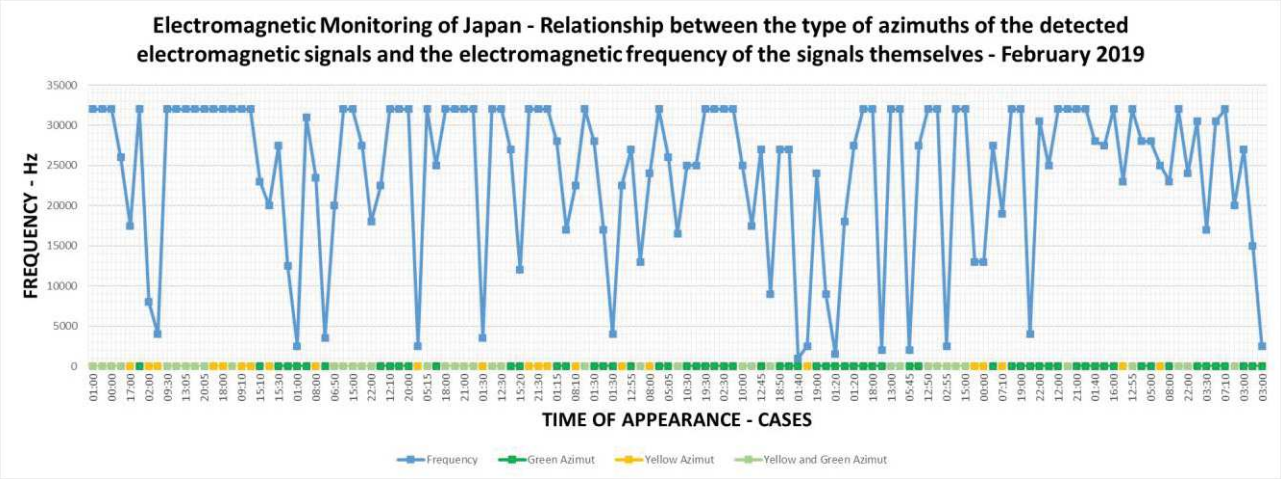

Fig 28 - Relationship between the electromagnetic frequency of the signals received and their azimuth of origin. (green, green / yellow, yellow). Source: Radio Emissions Project. February 2019.

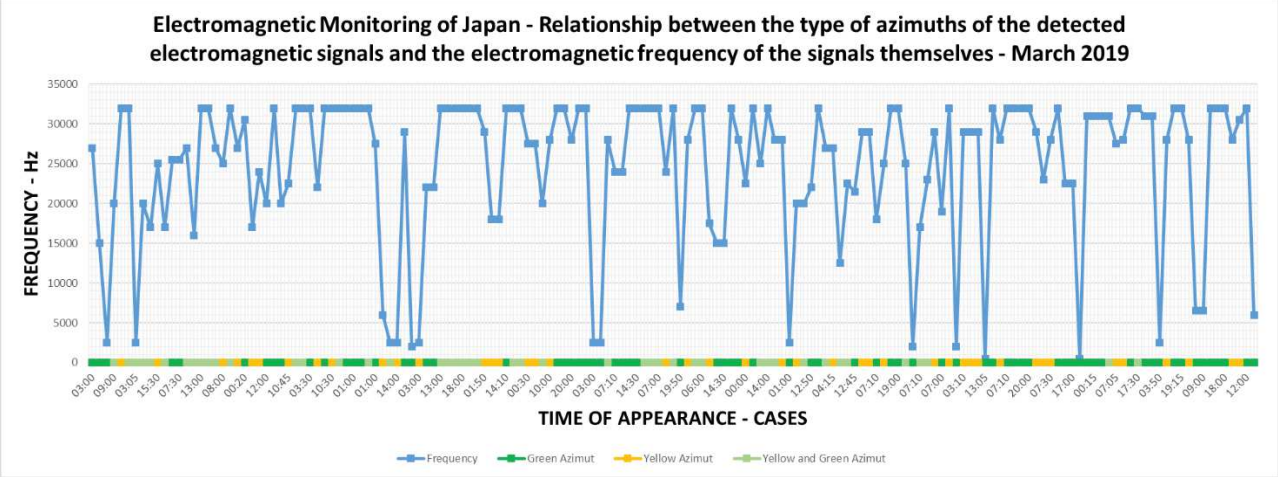

Figure 29 - Relationship between the electromagnetic frequency of the signals received and their source azimuth. (green, green / yellow, yellow). Source: Radio Emissions Project. March 2019.

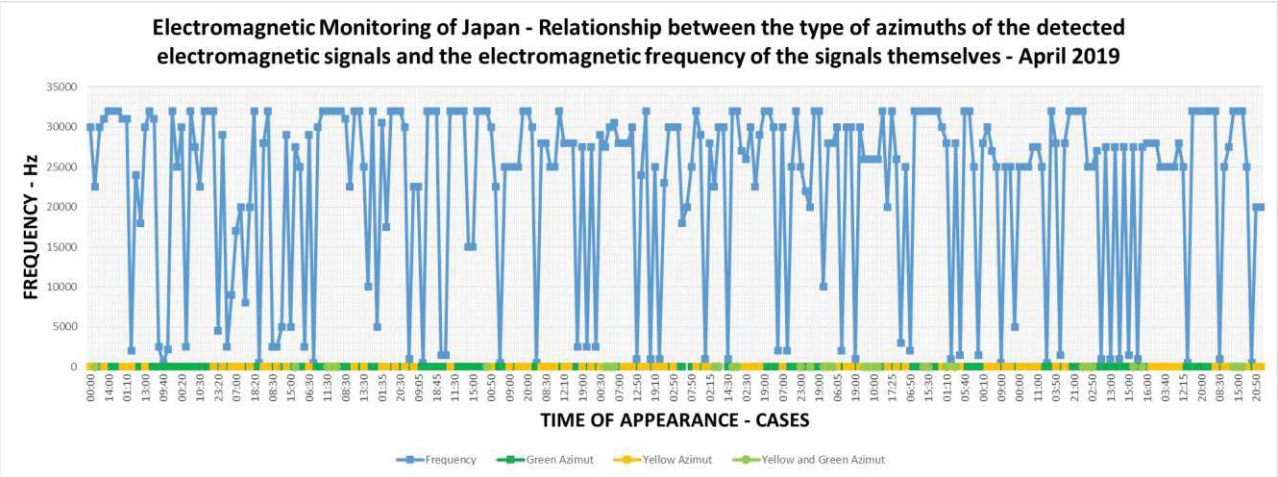

Figure 30 - Relationship between the electromagnetic frequency of the signals received and their origin azimuth. (green, green / yellow, yellow). Source: Radio Emissions Project. April 2019.

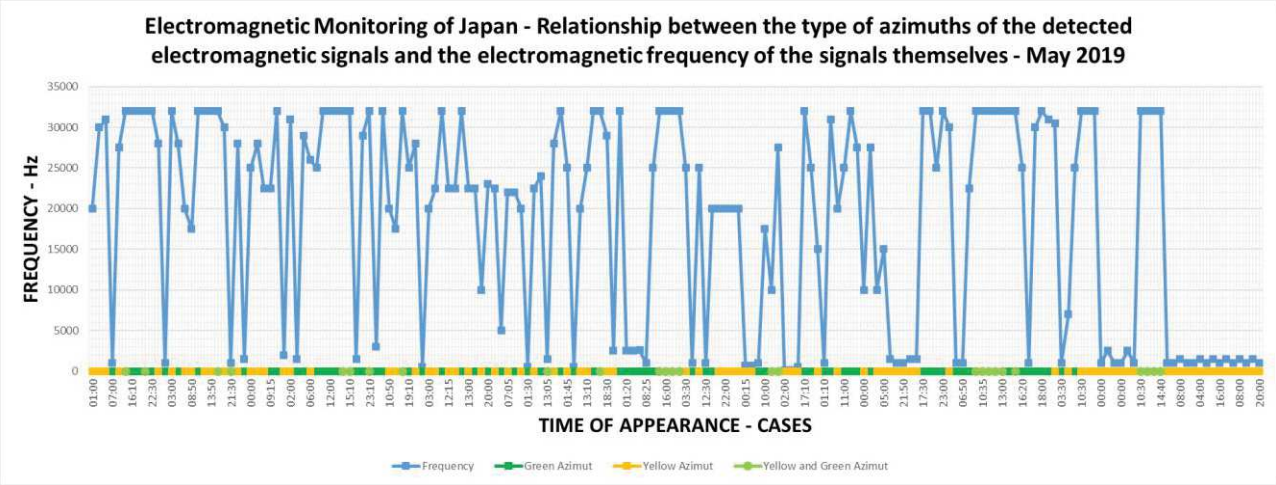

Figure 31 - Relationship between the electromagnetic frequency of the signals received and their origin azimuth. (green, green /yellow, yellow). Source: Radio Emissions Project. May 2019.

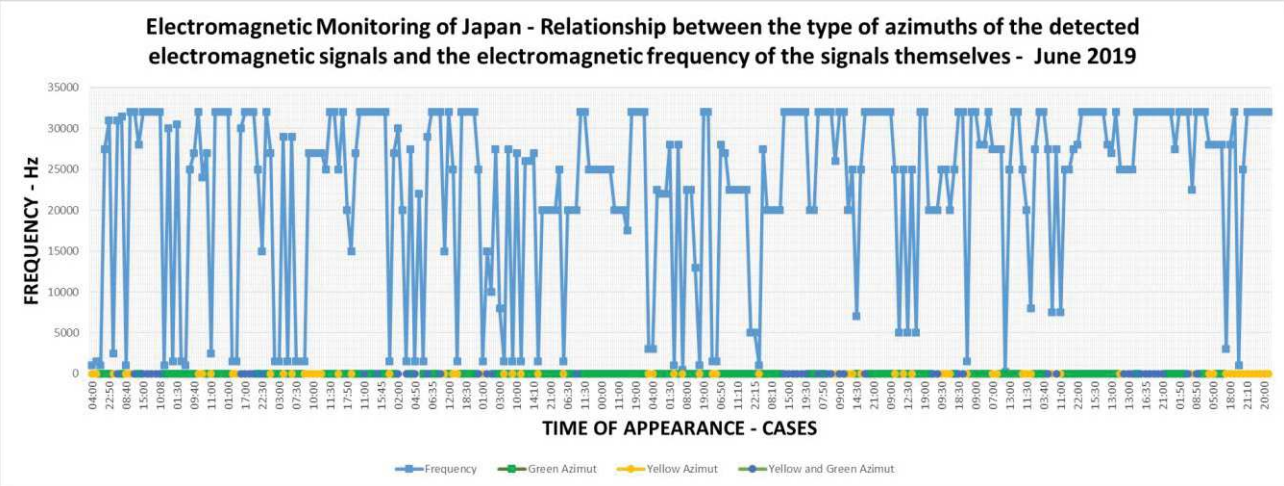

Figure 32 - Relationship between the electromagnetic frequency of the signals received and their source azimuth. (green, green / yellow, yellow). Source: Radio Emissions Project. June 2019.

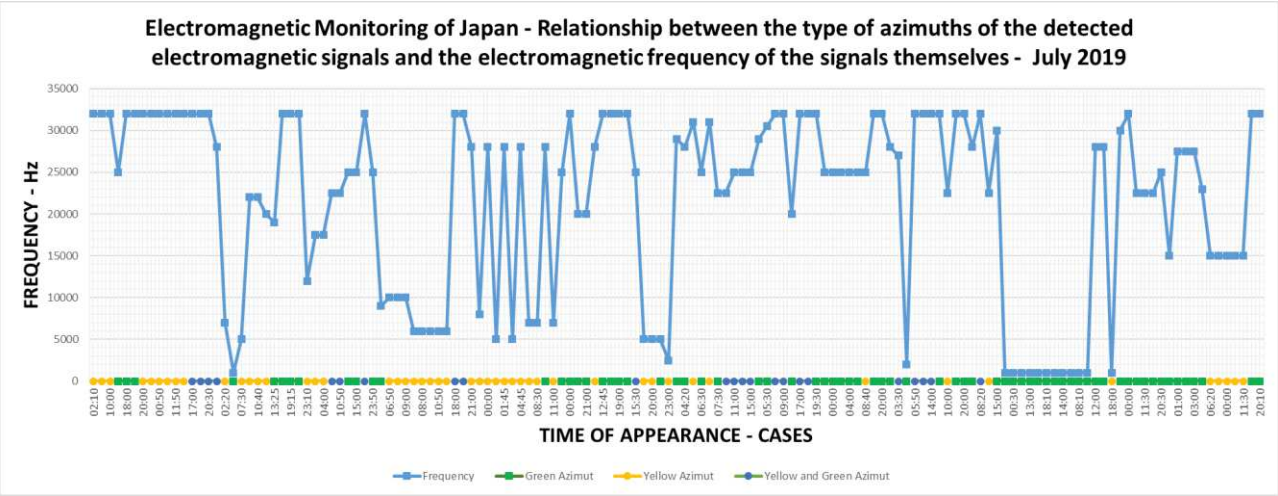

Figure 33 - Relationship between the electromagnetic frequency of the signals received and their azimuth of origin. (green, green / yellow, yellow). Source: Radio Emissions Project. July 2019.

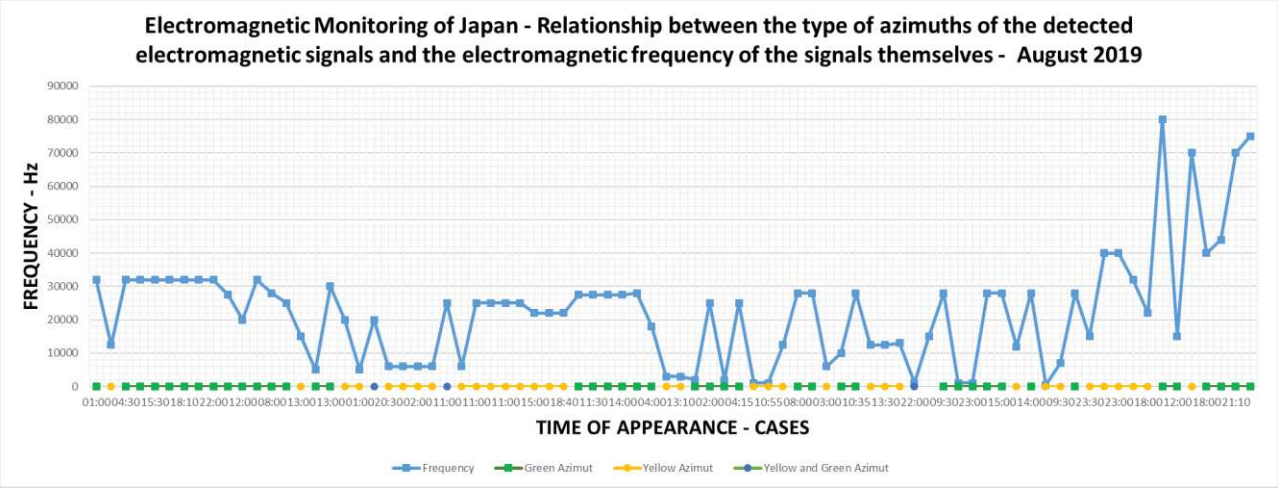

Figure 34 - Relationship between the electromagnetic frequency of the signals received and their source azimuth. (green, green / yellow, yellow). Source: Radio Emissions Project. August 2019.

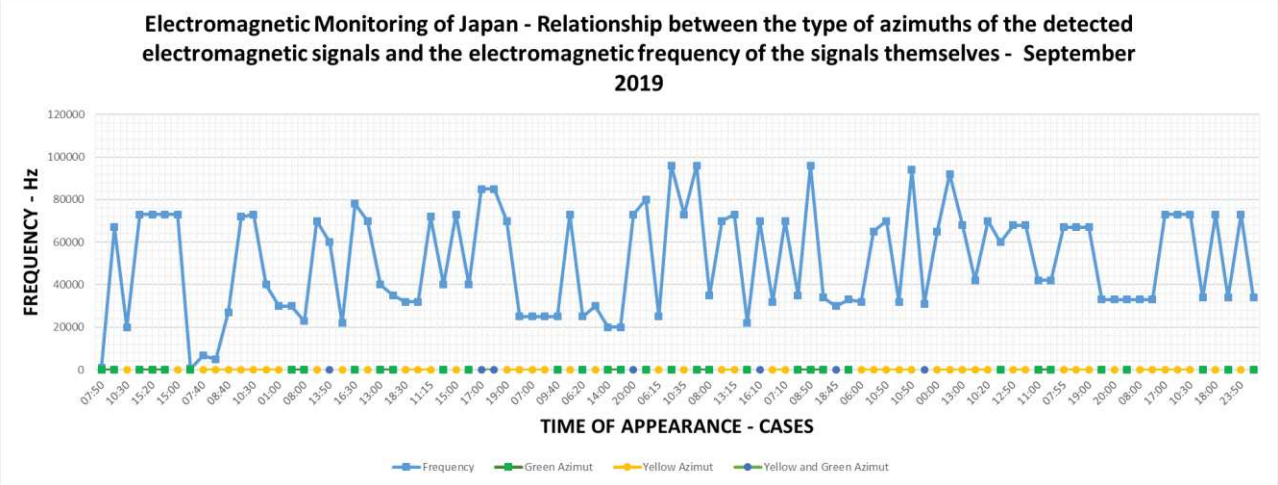

Fig. 35 - Relationship between the electromagnetic frequency of the signals received and their source azimuth. (green, green / yellow, yellow). Source: Radio Emissions Project. September 2019.

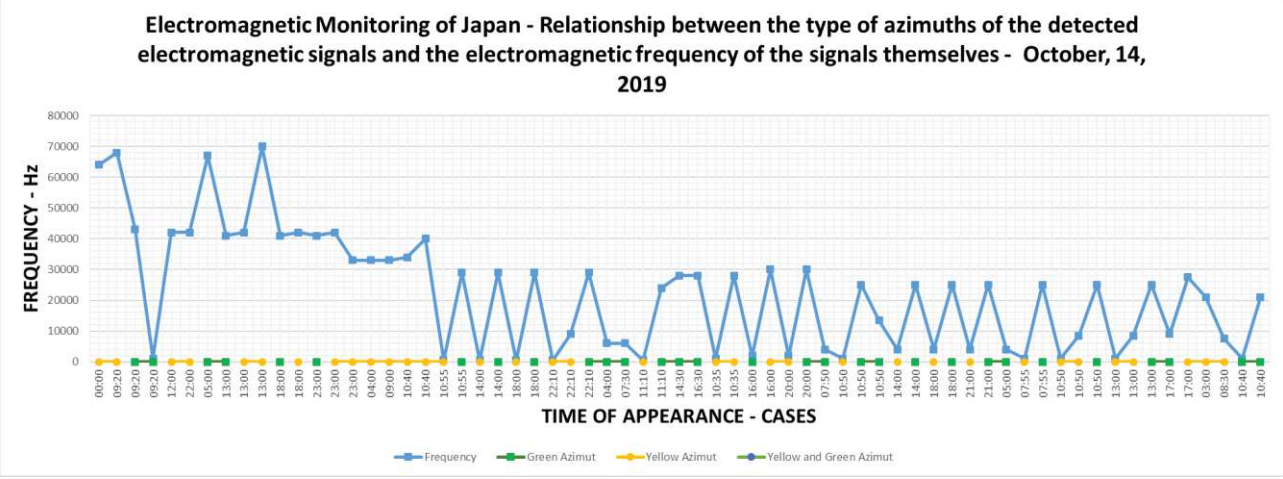

Figure 36 - Relationship between the electromagnetic frequency of the signals received and their azimuth of origin. (green, green / yellow, yellow). Source: Radio Emissions Project. October 2019.

The relationship between the electromagnetic frequency of the recorded signals and the distribution of the azimuths, from which these signals seem to come, is indicated by the graphs relating precisely to

the coloring of the azimuth and the peaks related to the electromagnetic frequency of the signals, extrapolated from the dynamic spectrograms in the study (as visible in Fig. 27, 28, 29, 30, 31, 32, 33, 34, 35, 36). In this case the yellow azimuth indicates the geographical center of Japan.

The relationship observed between the type of azimuth from which the electromagnetic signals seem to come and the distribution of Japanese earthquakes, tells us that the azimuth most commonly called is the yellow one, while many other appearances of electromagnetic signals seem to be those that come from the 'green azimuth. The data confirm that the signals from the Japanese area are those that seem to be generated in the direction of the center of this azimuth variation, which runs right in the center of Japan.

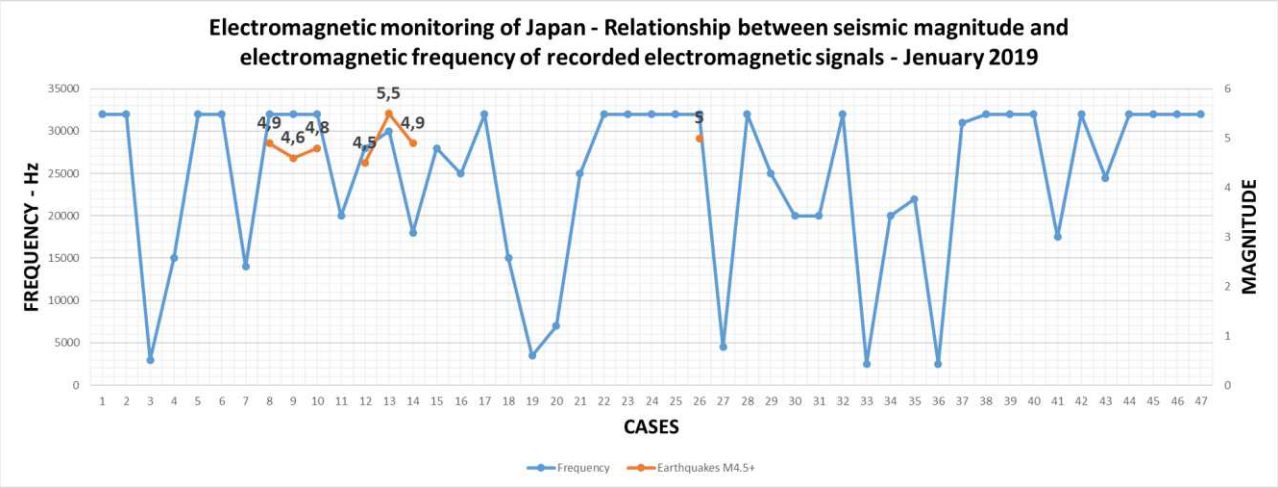

Fig. 37 - Relationship between the electromagnetic frequency of the signals received and the distribution of seismic events with magnitude M4.5 +. registered in January 2019 - Source Radio Emissions Project; USGS. January 2019.

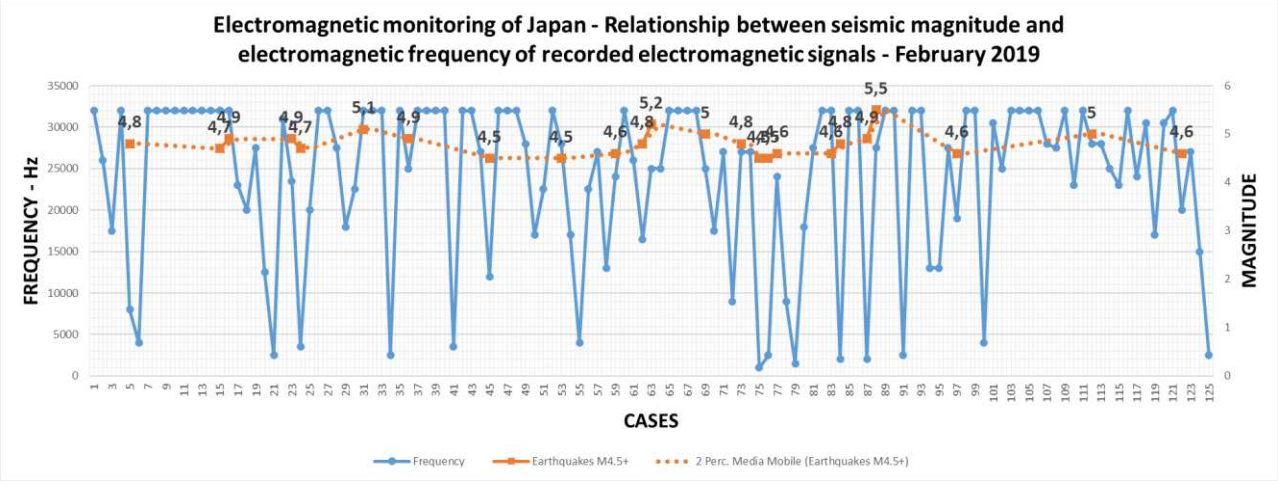

Figure 38 - Relationship between the electromagnetic frequency of the signals received and the distribution of seismic events with magnitude M4.5 +. registered in February 2019 - Source Radio Emissions Project; USGS. January 2019.

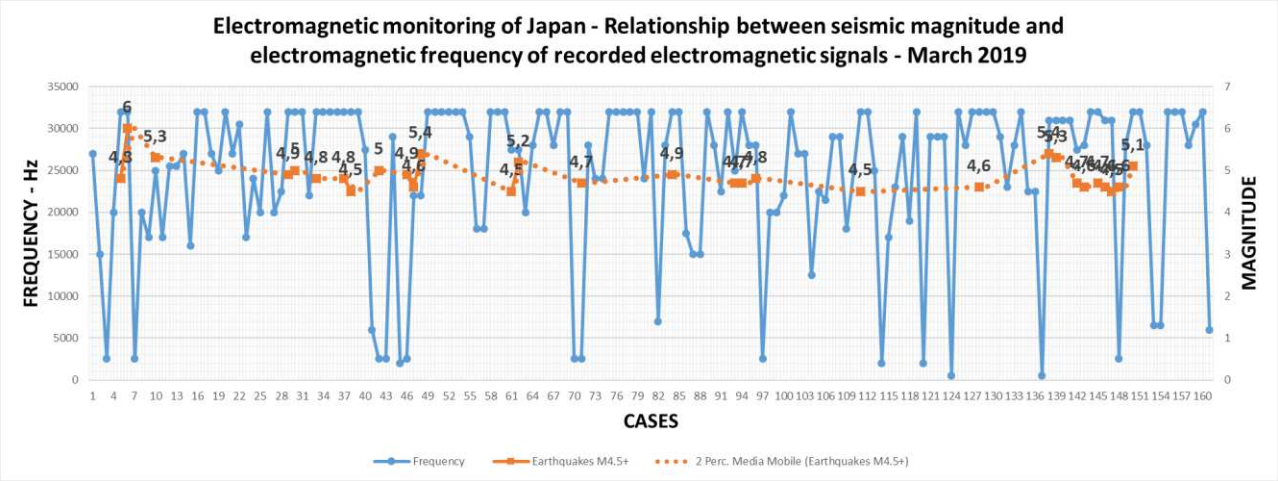

Figure 39 - Relationship between the electromagnetic frequency of the signals received and the distribution of seismic events with magnitude M4.5 +. registered in March 2019 - Source Radio Emissions Project; USGS. January 2019.

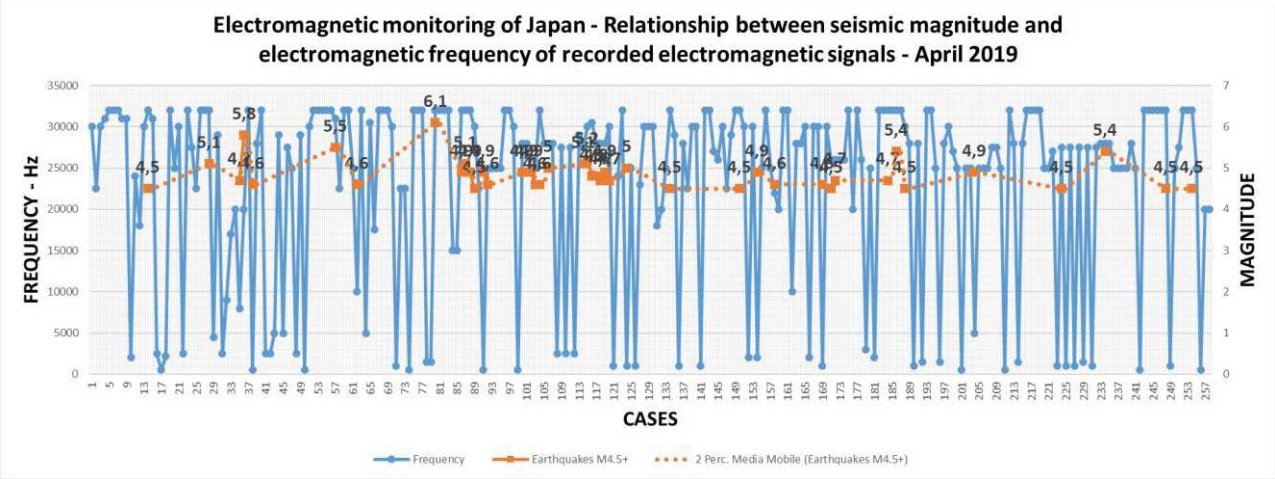

Figure 40 - Relationship between the electromagnetic frequency of the signals received and the distribution of seismic events with magnitude M4.5 +. registered in April 2019 - Source Radio Emissions Project; USGS. January 2019.

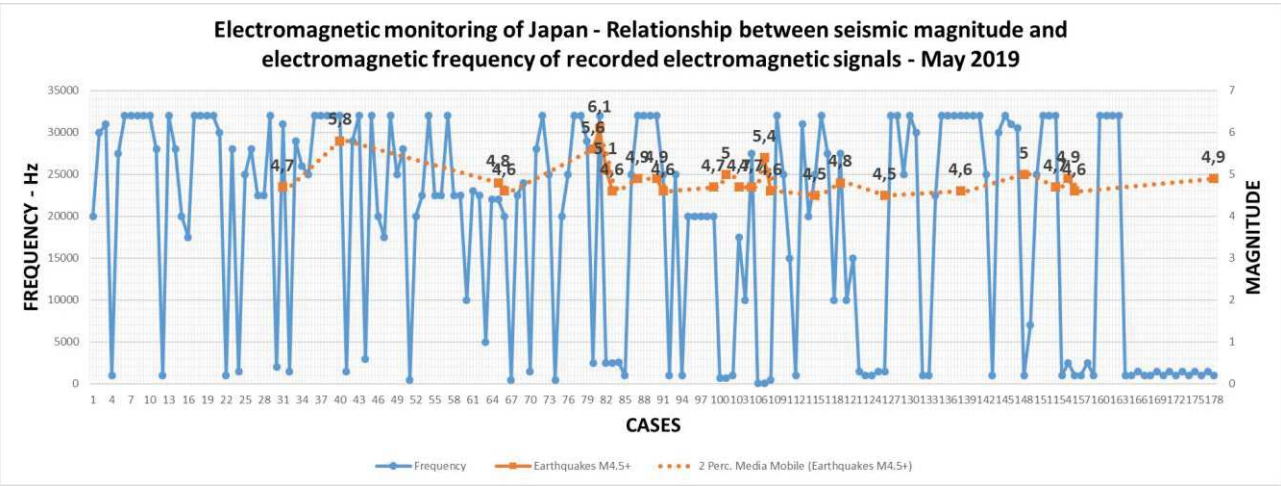

Figure 41 - Relationship between the electromagnetic frequency of the signals received and the distribution of seismic events with magnitude M4.5 +. registered in May 2019 - Source Radio Emissions Project; USGS. January 2019.

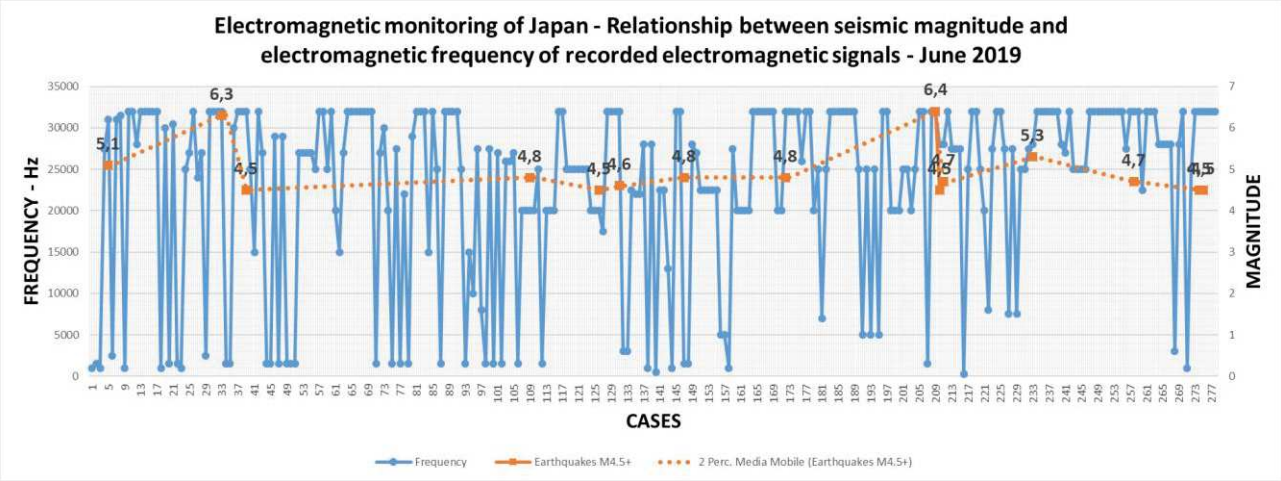

Figure 42 - Relationship between the electromagnetic frequency of the signals received and the distribution of seismic events with magnitude M4.5 +. registered in June 2019 - Source Radio Emissions Project; USGS. January 2019.

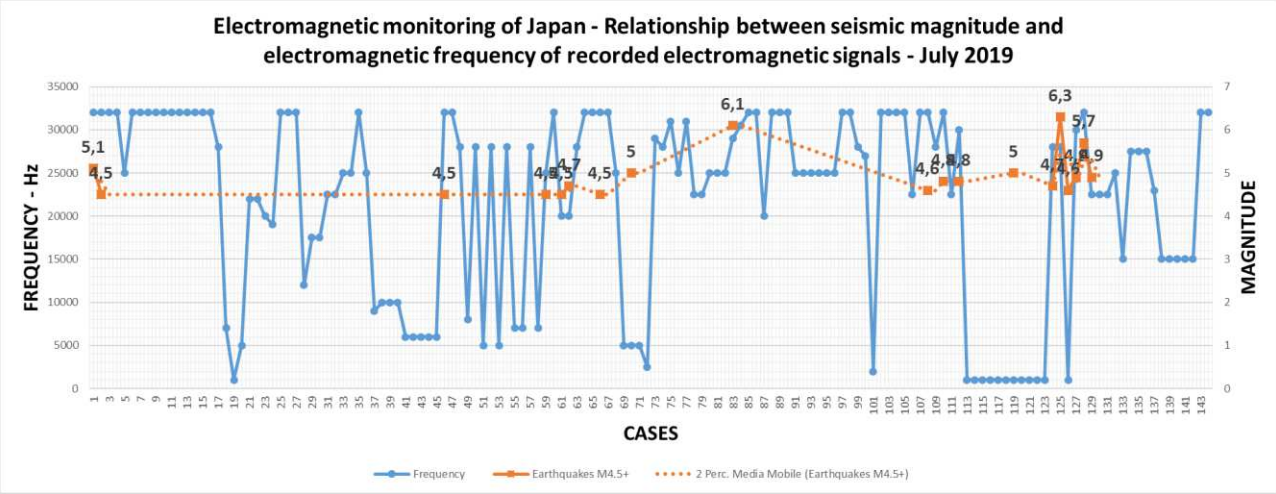

Figure 43 - Relationship between the electromagnetic frequency of the signals received and the distribution of seismic events with magnitude M4.5 +. registered in July 2019 - Source Radio Emissions Project; USGS. January 2019.

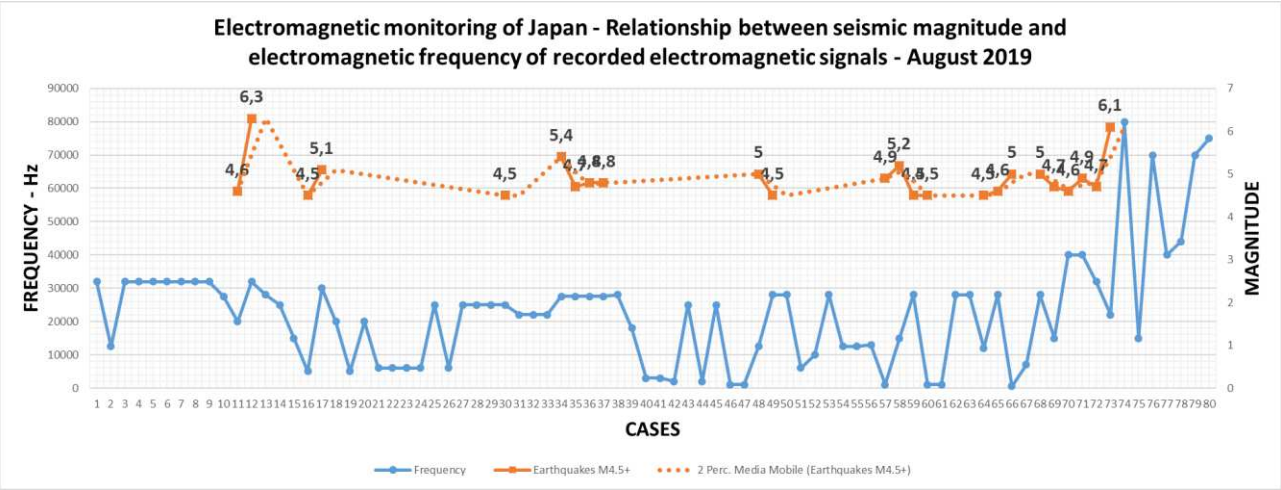

Figure 44 - Relationship between the electromagnetic frequency of the signals received and the distribution of seismic events with magnitude M4.5 +. registered in August 2019 - Source Radio Emissions Project; USGS. January 2019.

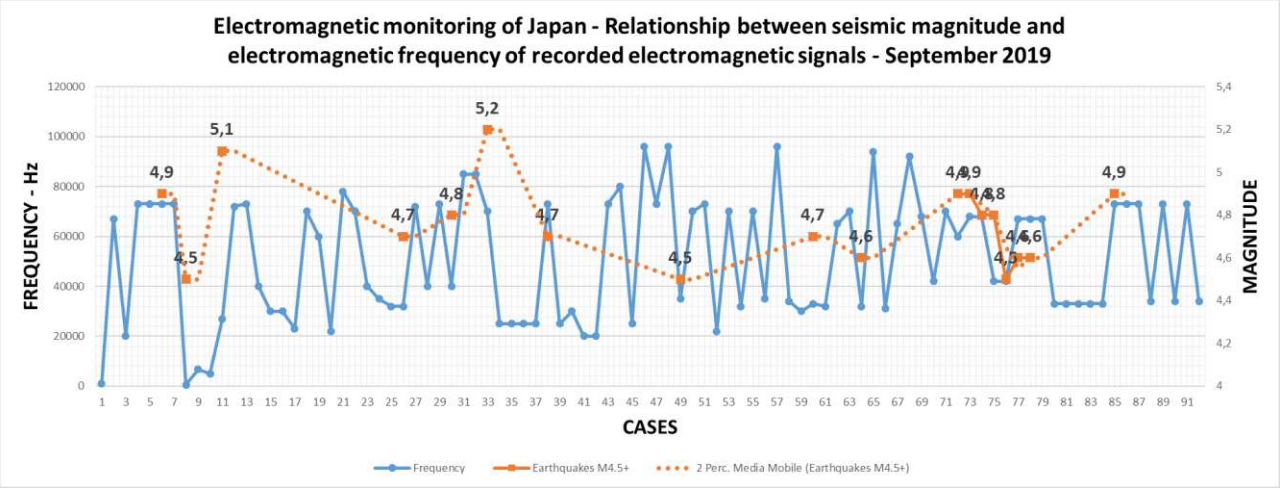

Figure 45 - Relationship between the electromagnetic frequency of the signals received and the distribution of seismic events with magnitude M4.5 +. registered in September 2019 - Source Radio Emissions Project; USGS. January 2019.

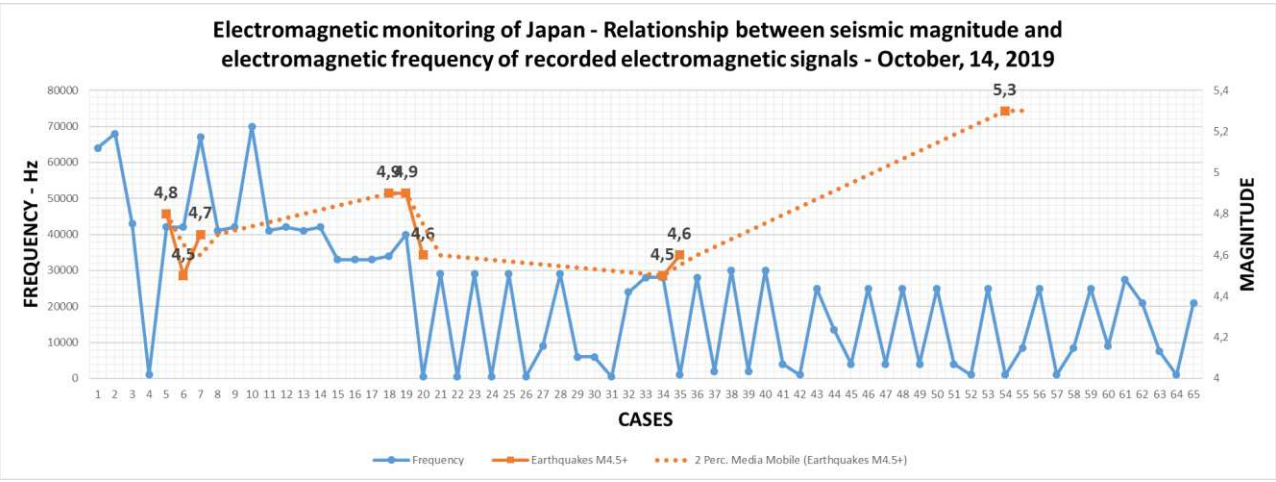

Figure 46 - Relationship between electromagnetic frequency of the received signals and the distribution of seismic events with magnitude M4.5 +. registered in October 2019 - Source Radio Emissions Project; USGS. January 2019.

The distribution of the electromagnetic frequency of the recorded signals, in relation to the temporal appearance of Japanese earthquakes with magnitude M4.5 +, indicates that seismic phenomena occur during electromagnetic increases that have appeared across the whole band (0-32 and 0-96 kHz), i.e. when the electromagnetic signals recorded by the RDF system are very extensive and exceed all other natural emissions present in the geomagnetic background (as visible in Fig. 37, 38, 39, 40, 41, 42, 43, 44, 45, 46) .

In this context, it is evident that the seismic magnitude follows the average frequency of the electromagnetic signals from the Japanese azimuth, in a directly proportional way. For the first time ever, the evidence from monitoring shows that there is a close relationship between crustal-type electromagnetic emissions and the occurrence of earthquakes of a certain magnitude.

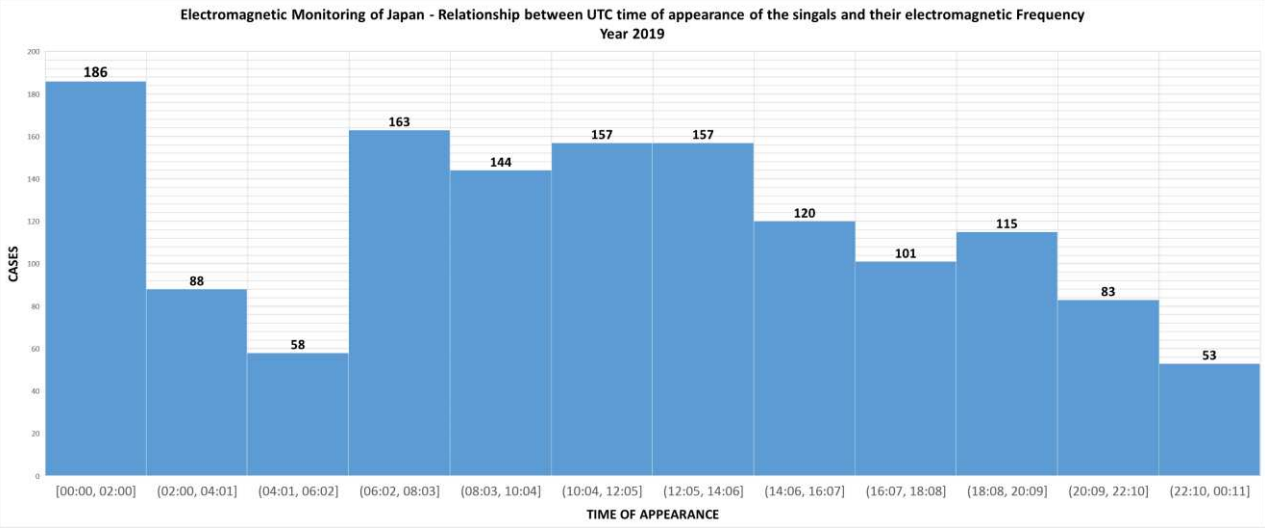

Figure 47 - Appearance of radio anomalies, with respect to the UTC time recorded by the RDF system developed by the Radio Emissions Project. The graph highlights well-distributed peaks and the number of radio anomalies associated with each group of hours considered within the study.

Scientific evidence shows that there are three substantial groupings of apparitions (electromagnetic signals - radio anomalies) well distributed, a first group is the one recorded between 00:00 UTC and 02:00 UTC, a second group is between 06:00 UTC and 14:00 UTC. A third and final grouping is found between 18:00 UTC and 20:00 UTC (Fig. 47).

The distribution of the hypocentral depth (Fig. 48) of the earthquakes that occurred in Japan, if related to the electromagnetic frequency of the radio-recorded anomalies by the RDF system, before the seismic events occurred, shows how, the deepest earthquakes were preceded by signals having an electromagnetic frequency distributed at a lower frequency, compared to earthquakes with a lower depth, preceded by signals distributed over the entire electromagnetic band.

As physics teaches us, the higher the frequency, the lower its propagation capacity through the planetary body, and vice versa. In this case, the data indicate precisely this phenomenon, where an electromagnetic frequency higher than the signals received before surface earthquakes have occurred.

This can be explained precisely thanks to the attenuation of the electromagnetic signal by the earth's crust: the greater the depth (in km), in which the electromagnetic emissions are generated, arising from local piezoelectric phenomena (electromagnetic dipoles determined by the distribution of electric charges, for the breaking of the crystalline lattice of rocks subjected to tectonic stress), and lower are the electromagnetic frequencies capable of reaching the ground level, to then be propagated in the earth-ionosphere cavity, and vice versa.

It will therefore be expected, as noted, that at a certain distance from these natural emitters (electromagnetic dipoles), the higher frequency emissions come from more superficially generated, therefore less attenuated, electromagnetic emissions, which are allowed to bounce off the ionospheric layers and reach thus far distant places, where they can then be received.

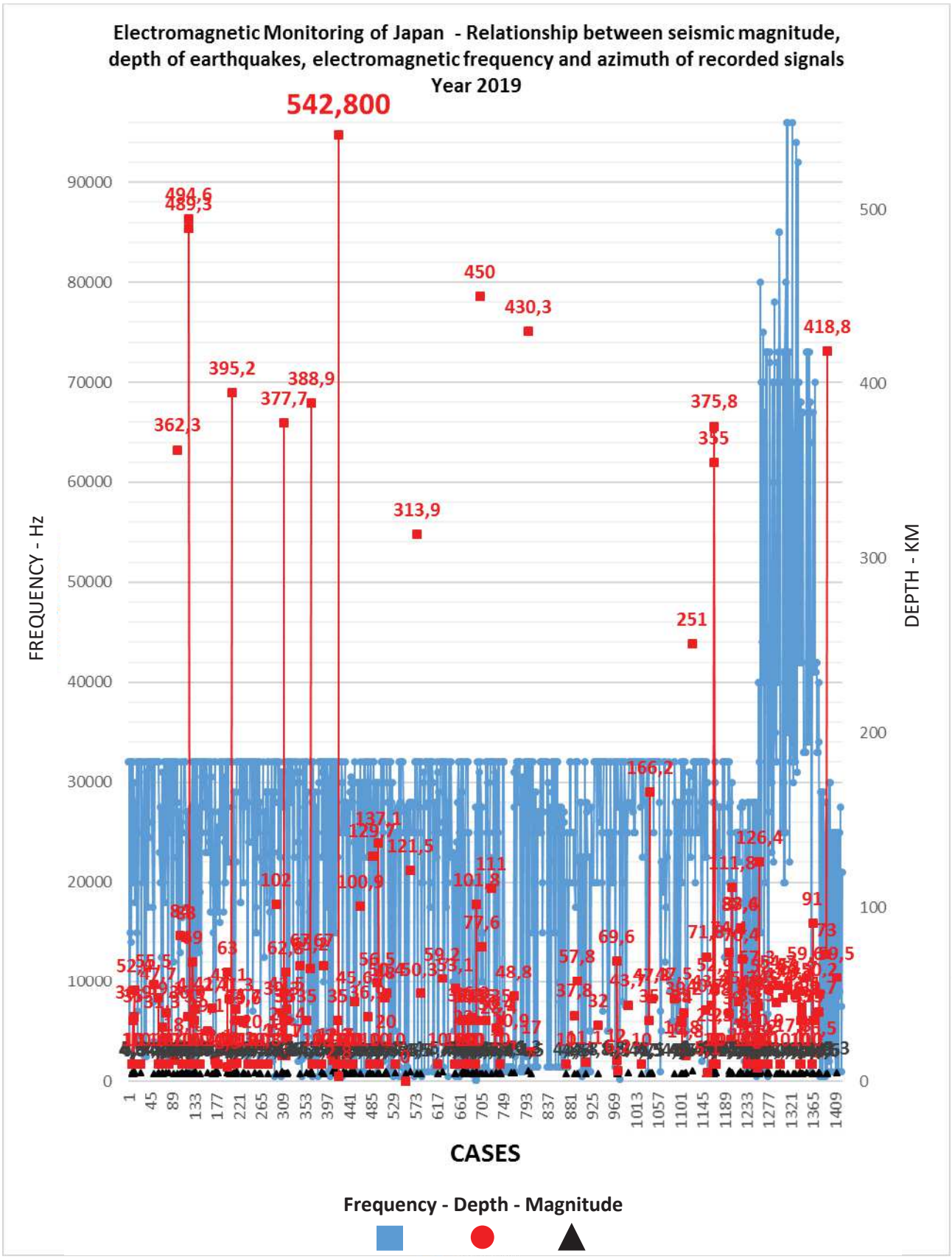

Fig. 48 - Relationship between the electromagnetic frequency of the recorded signals, the azimuth of origin in the direction of Japan and the distribution of the seismic events that occurred, with reference to their hypocentral depth and seismic magnitude. Source: Radio Emissions Project; USGS. Data from 2019.

6 – HYPOTHESIS

This important data strongly suggests that the emissions recorded by the monitoring system originated at the crustal level (in depth), precisely because the frequency distribution of the radio anomalies, compared to the seismic depth, shows that they follow the attenuation rules of propagation, better known as "fading by diffraction", due to the presence of physical obstacles, which in this case are represented by the layer of rocks in depth, just above the point where these signals are generated which acts as a filter, letting escape via the lower frequency electromagnetic frequencies, compared to those with higher frequency, depending on the depth of the emission point.

In this case even if these signals, to be detected thousands of kilometers away, seem to possess enormous powers in Watts, they do not only go to dissipate as a result of the "fading from soil reflection" which produces reflected waves which then go to added, with different phases, to the main wave, creating interference and random evanescence similar to "multipath fading", but in this case, thanks to seismic data, we know that this drop in frequency is associated with a lower seismic depth. Indicates that the lowering is substantially due to the depth of the electromagnetic emission in km, and not to the ionospheric fading phenomena.

In the face of this discovery, following the frequency characteristics of electromagnetic emissions, it is possible to partially understand their emission depth.

As regards instead the "phase shift" of the azimuth of the recorded signals (error in degrees with respect to the distance of origin of the signals themselves), we can certainly assume that this depends on the "multipath fading" which is a form of distortion of the electromagnetic signal which reaches its destination in the form of a certain number of replicas, out of phase over time, originating from the various paths (multipath) that the signal itself may have undergone during its propagation and summing up to each other in reception; moreover, each replica, having made its own path of a certain length and characterized by a different reflection on generally different surfaces, will therefore be subject to an attenuation in general different from that suffered by the other replicas. It is a typical problem of both fixed and mobile radio communications in a deterministic manner in the first case and with characteristics typical of a random process in the second case.

This would explain the azimuth error observed at a great distance, compared to the emissions coming from a few tens of kilometers away from the RDF detection station. These hypotheses are supported by the studies conducted by our team starting from 2017 (Straser et al., 2018).

7 – CONCLUSIONS

The data acquired with the RDF system have shown how it is possible to identify the direction of arrival of natural electromagnetic signals, and predict, with some precision when an earthquake can occur, along the azimuth indicated by the monitoring system.

In this context, the system if implemented can provide important information of a predictive nature in the field of seismogenesis, as well as providing suggestions on the evolution of the phenomena interconnected with the seismogenic phenomena that are at the basis of the seismic trigger. It is the duty of researchers to proceed along this field of research and invest efforts and economic funds for the realization of an integrated RDF system, even of a multiparametric type, that is, capable of correlating several types of data together.

REFERENCES

Cataldi, G., Cataldi, D., Rossi, R. and Straser, V., 2016. SELF-ELF Electromagnetic signals correlated to M5+ Italian Earthquakes that occurred on August 24, 2016 and January 18, 2017. NCGT Journal, vol. 5, no. 1, p. 134-143.

Cataldi, D., Cataldi, G. and Straser, V., 2017. SELF and VLF electromagnetic emissions which preceded the M6.2 Central Italy earthquake that occurred on August 24, 2016. European Geosciences Union (EGU), General Assembly 2017. Seismology (SM1.2)/Natural Hazards (NH4.7)/Tectonics & Structural Geology (TS5.5). The 2016 Central Italy Seismic sequence: overview of data analyses and source models. Geophysical Research Abstracts Vol. 19, EGU2017-3675.

Furumura T., Takemura S., Noguchi S., Takemoto T., Maeda T., Iwai K., Padhy S., 2011. Strong ground motions from the 2011 off-the Pacific-Coast-of-Tohoku, Japan (Mw = 9.0) earthquake obtained from a dense nationwide seismic network - Landslides, September, 8:333.

Straser, V., Cataldi, G. and Cataldi, D., 2015. Radio-anomalies: a tool for earthquake and tsunami forecasts. European Geosciences Union (EGU) General Assembly 2015, Natural Hazard Section (NH5.1), Sea & Ocean Hazard - Tsunami, Geophysical Research Abstract, vol. 17, Vienna, Austria. Harvard-Smithsonian Center for Astrophysics, High Energy Astrophysics Division, SAO/NASA Astrophysics Data System.

Straser, V., Cataldi, G. and Cataldi, D., 2016. SELF and VLF electromagnetic signal variations that preceded the Central Italy earthquake on August 24, 2016. NCGT Journal, vol. 4, no. 3, p. 473-477. Harvard-Smithsonian Center for Astrophysics, High Energy Astrophysics Division, SAO/NASA Astrophysics Data System.

Straser, V., Cataldi, G. and Cataldi, D., 2017. Seismic signals detected in Italy before the Nikol'skoye (off Kamchatka) earthquake in July 2017. NCGT Journal, vol. 5, no. 3, p. 391-396.

Straser V., Cataldi D., Cataldi G., 2018. Radio Direction Finding System, a new perspective for global crust diagnosis. New Concepts in Global Tectonics Journal, v.6, no. 2, June, p. 203-211.